Computational Polarization 3D - Monocular Shape Recovery from Non-Lambertian Object

Fatai Olarinde JIMOH

Master in Computer Vison
University of Burgundy

Under the Supervision of Prof. Christophe STOLZ
VIBOT ERL CNRS 6000 / ImViA, Université de Bourgogne

A Thesis Submitted for the Degree of
MSc in Computer Vision (VIBOT)
· 2022 ·

Abstract

Polarization application is an essential approach to recover shape information. This thesis aims at recovering surface shape from a non-Lambertian object with a single view. A non-Lambertian object consists of diffuse and specular reflection which can make it difficult for accurately recovering the surface shape. Another issue is addressing azimuth ambiguity during surface reconstruction which has been a major problem in shape from polarization. Based on these issues, the thesis proposes a monocular 3D polarization imaging approach by determining the subtle difference in the mixed reflection and then separating them using Independent Component Analysis (ICA). The separated pure diffuse reflection allows more accurate extraction of polarization properties based on which a gradient field is derived to estimate surface normal. The ambiguity is addressed by computing an optimization problem with a reference gradient field.

Table of Contents

List of Figures

Acknowledgement

All thanks to **God** for his blessings and grace, and for giving me the endurance, courage and strength during my studies and writing this thesis.

It is a great pleasure to acknowledge my deepest thanks and gratitude to my supervisor **Prof. Christophe STOLZ** for his patience, guidance, understanding and support during the course of this thesis. I am so grateful and it is a great honour to work under his supervision.

I would like to express my deepest gratitude to **Prof. David FOFI**, **Miss Sylvia** and **Mrs. Herma** for being there for me from the beginning of my journey in this course. I will forever be grateful because they all stood by me with their words and presence, and always telling me it is possible when I almost lost it. It means everything to me.

I am glad to mention **Prof. Fabrice Meriaudeau** and the ImViA Lab Director **Prof. Omar TAHRI** for their constant checkup during my thesis. Also, Joaquin **RODRIGUEZ**, **Devesh ADLAKHA** and **Mr. Yohan** for their well wishes always.

I would like to extend my gratitude to all my colleagues and friends particularly **Abdulateef ADERINOYE**, **Divine BAKALA**, **Walid BRAHIM**, **Rilwanu AR ROIYYAAN** and **AbdulMuiz** for their remarkable support and love during my studies. I wish them all the best in their future endeavours.

To **my Parents**, I dedicate this thesis to them for their hard work, love and prayers. They gave me the best they could from the very little they have. I am so blessed to have such caring parents who think about their children before themselves. I pray they live longer and see me and **my Siblings** excel in life.

I am blessed with amazing friends, always there to put smiles on my face during this course, **Ali Nair**, **Ayoub**, **Warren**, **Brahim**, **Abdulsalam**, **Anneke**, **Fabio**, **Tolu** and of course all the **CROUS staff** in Le Creusot for their care and support. I am so grateful for every single support from them all and I wish them all the best.

Finally, to everyone I did not mention that supported me directly or indirectly during this journey. I will not take your support for granted.

Chapter 1

Introduction

1.1 Overview

The importance of computer vision goes collectively with its application in the real world. Computer Vision is an interdisciplinary field that allows systems and computers to obtain resourceful information from digital images, videos and other forms of visual input. Shape information is important in 3D computer vision in respect to facial recognition applications and city modeling **[1-3]**. One of the fundamental problems in computer vision is retrieving 3D information about our surroundings. Human and animal can easily perceive objects with different shapes and appearance, but it is a serious task in computer vision.

Over the past few decades, both industrial and academics researcher have been determined and committed to develop algorithms in order to make machines able to sense and produce wide range of applications. For example, inventing robots that can perform human action particular helping to ease human life such as autonomous driving which aim is to enhance human driving efficiency while perceiving different traffic, road condition etc. Logistic robots can transport goods and manage store house to save lots of human resources. Rescue robots can go into risky and complicated environment where humans cannot safely reach. All these related tasks involve an elementary problem: that is, how to retrieve the data from our 3D world. Different sensors and technique have been developed to address this problem.

This thesis focuses on 3D shape reconstruction from polarization images. Polarization images records polarization state at each pixel of the image **[4].** Computational polarization vision aims to utilize this information for the purpose of tackling computer vision tasks.

This is an innovative technology, with the idea to provide new approaches to computer vision problems and future applications. Then again, there have been numerous applications exploiting polarizations in our daily life. For instance, you might experience that while diving or taking a walk on a sunny day, the dazzling illumination will blind one's view but by putting on a pair of polarized sunglasses, glare will be removed and the view becomes clearer. Another instance could be, trying a take a photo of a scene under a river and the scene under the river is mantled by the reflected light. By mounting a polarizing filter on the camera and adjusting it, you can see and capture a clearer view under the water Surface. An example is shown in Figure (1.1). There are so many other essential applications developed by the use of polarization such as 3D stereo movies, Liquid Crystal Display etc.

(a) Source : https://www.misterspex.co.uk/sunglasses-guide/sunglasses-lenses

(b) Source : http://www.paddling.net/sameboat/archives/sameboat496.html

Figure 1.1: Daily life polarization application (a) left image depicts a glare light scene without wearing sunglasses and right image depicts wearing sunglasses. (b) The left image depicts a photo captured without polarizing filter and the right depicts a photo captured with polarizing filter.

Polarization information can be computed from polarization properties of the reflected light since the shape of that object changes the polarization state of the reflected light **[5].** The polarization state of light reflected from non-metallic (dielectric) objects carries information about both the shape of the object and material properties **[6]**. The idea for this phenomenon is that unpolarized light becomes partially polarized when it is reflected diffusely through surface scattering **[7]** or specularly **[8]**. The orientation and degree of polarization correspondence to the local surface orientation, the refractive index of the material and reflectivity whether specular or diffuse. For an image captured by conventional camera; this information is not visible in the image. Such information becomes available if using either a custom polarization camera or mounting a rotating linear polarizing filter in front of the conventional camera.

A polarization camera captures supplementary information about the surface orientation of an object. These surface attributes can effectively improve methods that only uses intensity information. As such;

a) With a proper formulation, it can achieve the separation of diffuse and specular reflection which will be addressed in this thesis.
b) It gives surface normal information on regions that are featureless where stereo matching fail.
c) On pixels with high specularity and inter-reflection, detailed reconstruction is possible while shape from shading and multi-stereo fail.

1.2 Problem Statement

In recent years, different methods, such as time of flight (TOF), structured light illumination, binocular stereo imaging, and laser radar (LIDAR), have been developed **[9-12]**. However, these methods are quite complex because it requires special illumination or multi viewpoints. Retrieving shape information can also estimate using polarization properties. The 3D reconstruction technique of shape from polarization avoids some

limitations in other method as such, multi viewpoints, active pattern illumination, high-speed detector etc.

The procedure to acquire shape from polarization rely on specular or diffuse reflections from the object. However, the reflection of light from many objects consists of diffuse and specular reflection components **[13]**. The uneven distribution of specular reflection will lead to a non-unique normal direction; therefore, efforts have been made to recover shape from diffuse polarization.

This thesis addresses recovering shape information from a non-Lambertian object with a single view. A non-Lambertian object contains the presence of both specular and diffuse reflection. Accurate shape recovery of an object with mixed reflection (non-Lambertian) requires polarization properties from a purely diffuse reflection since the light incident is not sensitive to a direction and it distributes evenly on the whole surface than specular reflection. Therefore, it is essential separate the specular reflection from the mixed reflection.

However, the thesis first addresses the major obstacle of mixed reflection on the non-Lambertian surface by finding the subtle difference in polarization between diffuse and specular reflection and then separating them by using Independent Component Analysis (ICA) algorithm, and addresses the azimuth ambiguity during surface reconstruction.

1.3 Objectives

The goal of the project is to present a monocular 3D imaging method using polarization properties of the reflected light from a non-Lambertian object and the objectives are:

1. To address the major obstacle of the mixed reflection on the object surface by separating the specular reflection from the mixed reflection in order to obtain a pure diffuse image.
2. To address the azimuth ambiguity during the surface reconstruction.

1.4 Thesis Outline

This remainder of the thesis is organized as follows:

- **Chapter 2. State of the Art:** This chapter describes the basic theory of polarization of light and explains the derivation of the polarization reflectance model which is widely used in Computer Vision. Finally, then did review of different method involved with shape estimation and reconstruction.
- **Chapter 3. Methodology:** This chapter presents the Research Methodology which includes the proposed method and implementation.
- **Chapter 4. Results:** This chapter shows the results obtained with detailed analysis and conclusion in;
- **Chapter 5. conclusion and perspectives:** This chapter gives the summary of the thesis is concluded as well as suggestion for future proposal.

Chapter 2

State of the Art

This chapter reviews the theoretical background related to polarization of light and explains how to derive polarization reflectance models. Finally, discussed some methods for shape estimation and reconstruction.

2.1 Polarization phenomenon

Polarization of light is an important topic of discussion in physical science particularly in optics and photonics applications. The idea behind this theory was developed to give a better understanding of the phenomenon between n the interaction of light and matter.

In 1669, the first idea of the existence of polarized light surfaced when *Erasmus Bartholin* discovered double refraction of a light ray. He disclosed that calcite crystals produce a double image when an object viewed through the crystal in transmitted light **[14].** Bartholin further discovered an unusual phenomenon during his experiment that when the calcite crystals are rotated about an axis, one among the images moves in a circle around the other which deduced strong evidence that the crystals somehow split the light into two different beams.

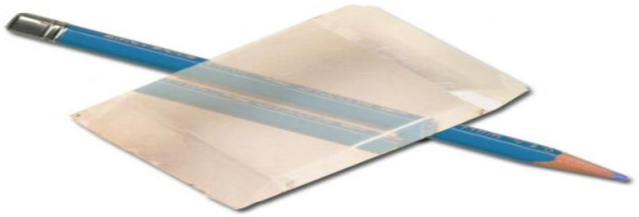

Figure 2.1: Bi-Refraction in Calcite Crystals (picture source: Nikon Instruments Inc. 2022)

A Dutch physicist *Christiaan Huygens* further discovered that by allowing these two lights passes through a second calcite crystal, and rotating it, the intensity of one ray was maximized while the other disappeared. At 45^{o} rotation, the intensities of these rays were equal. About a century later, a French physicist *Etienne Malus* experimented with images made with light reflected through calcite crystals and discovered that one of the images will vanish under certain circumstances **[14].** He made a correction on the fact that ordinary daylight comprises two different light forms that were passed through the calcite crystals in separate paths. It was later confirmed that such difference occurs due to the polarity of the light that passed through the crystal. The natural sunlight is composed of light vibrating in all planes, while reflected light is constricted often to a single plane which is parallel to the surface from which the light is reflected.

In the early 19th century, *Augustin-Jean Fresnel* proposed his theory called Fresnel's wave theory in order to explain this phenomenon of light. *Fresnel and Arago* further experimentally discovered that the optical field can be broken down to two orthogonal components in the plane transverse to the direction of propagation **[15]**. The component of electric field polarized parallel to the incident plane is called *p-polarized* while the component of electric field polarized perpendicular to the incident plane is called *s-polarized* as shown as E_x and E_y respectively in Figure (2.2).

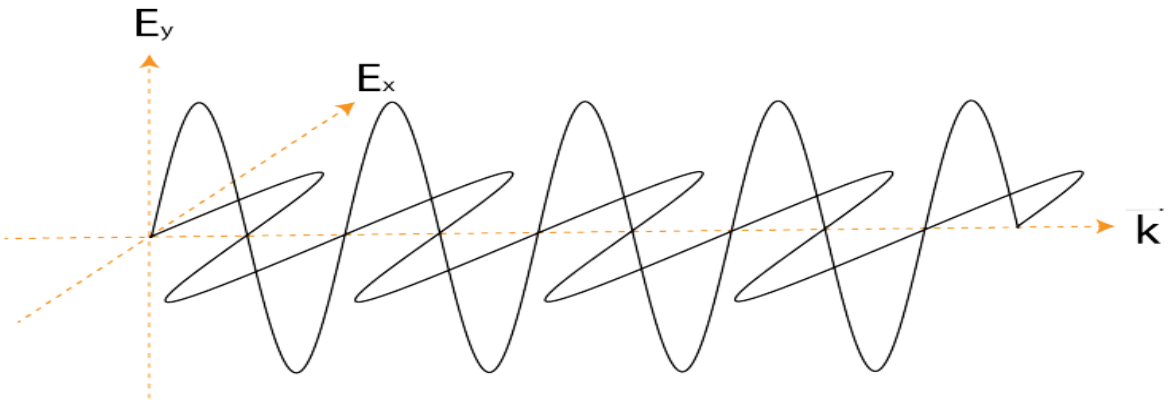

Figure 2.2: illustrates two orthogonal waves assuming the plane of our paper is the incident plane. E_x is *s-polarized* while E_y is *p-polarized* component.

Natural sources such as sunlight, as well as artificial sources give rise to light. The light is known as a wave phenomenon which can interact with surfaces through reflection, transmission and scattering (or diffraction) as shown in Figure (2.3). These interactions depend on the physical properties of the material, the wavelength of the incident radiation and angle of reflection. A light reflected from a flat surface of an insulating material (or dielectric) is often partially polarized. Examples of such surfaces that reflect polarized light are glass, undisturbed water, sheet plastics etc. with the electric vectors of the light reflected moving in a plane that is parallel to the surface of the material. The exact amount of reflected light that is polarized is determined based on the optical properties of the insulating material. One of the main properties of reflected light is that the degree of polarization is subjected to the incident angle of the light with an increase in polarization being observed for decreasing incident angle.

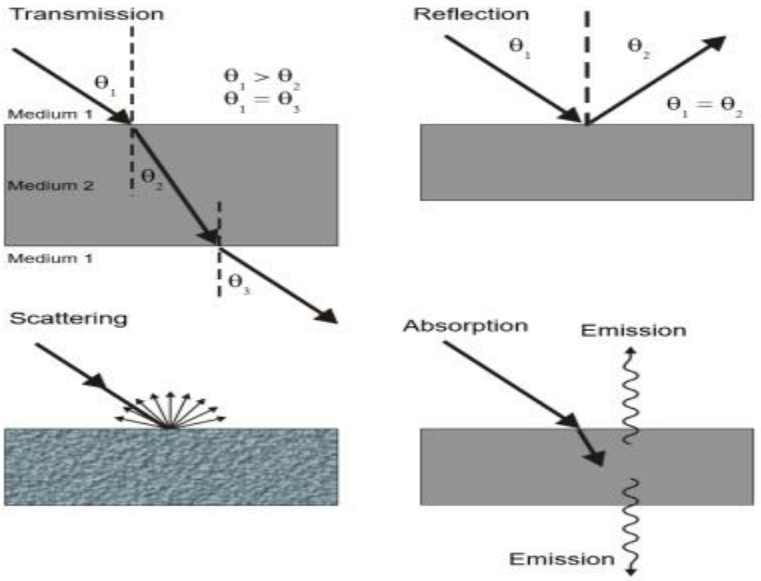

Figure 2.3: Light interaction (picture source: Olsen p.45)

When the direction of light is well defined for a given period, polarization comes to mind; the state of polarization is the most common feature of an electromagnetic wave.

Polarization describes how an electric field moves and has directional characteristics as such, the light is said to be polarized because the electric field oscillates in a direction. This

wave goes through the vacuum to reach us and prior to Earth's magnetic field, it becomes an Electromagnetic wave.

2.1.1 Type of Polarization

The polarized light can be classified into three types of polarization depending on how the electric field is oriented.

2.1.1.1 Linear Polarization

Light is said to be linearly polarized if the oscillation of the electric field vector is restricted to a single plane along the direction of propagation. It occurs when two orthogonal planes have the same phase but different amplitudes possibly. The transverse electric field wave is accompanied by a magnetic wave as illustrated in Figure (2.4).

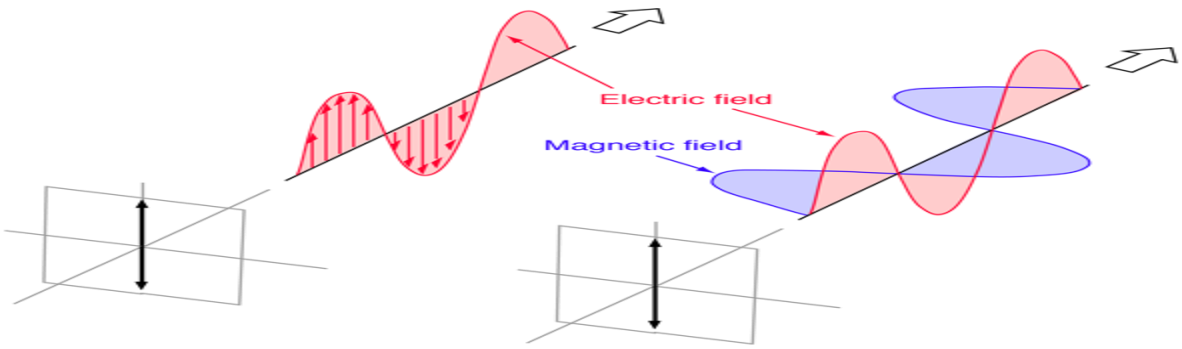

Figure 2.4: Linear Polarization (Picture source: HyperPhysics Website)

2.1.1.2 Circular Polarization

This is a polarization when at every point the electromagnetic field has a constant magnitude and its direction rotates with a constant value in a plane perpendicular to the direction of the wave. The electric field of the light consists of two perpendicular plane waves of equal amplitude but have a phase difference of $\pi/2$. The resulting electric field can rotate in two ways depending on the rotation direction. If the electric vector of the light

rotates anticlockwise, the light is said to be right-circularly polarized and if the electric vector of light rotates clockwise, then it is said to be left-circularly polarized. The illustration Figure (2.5) shows a right-circularly polarized.

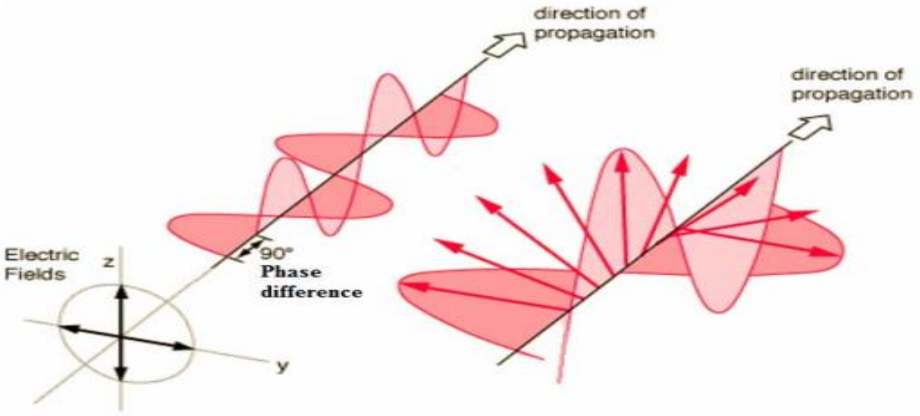

Figure 2.5: Circular Polarization (Picture source: HyperPhysics Website)

2.1.1.3 Elliptical Polarization

In elliptical polarization, the electric field describes an ellipse. The electric field consists of two linear components that are perpendicular to each other with different amplitudes and/or their phase difference is not $\pi/2$. Elliptical polarization (Figure 2.6) is the most general definition of polarized light. Linear and circular polarized light can be considered special cases of elliptical polarized light.

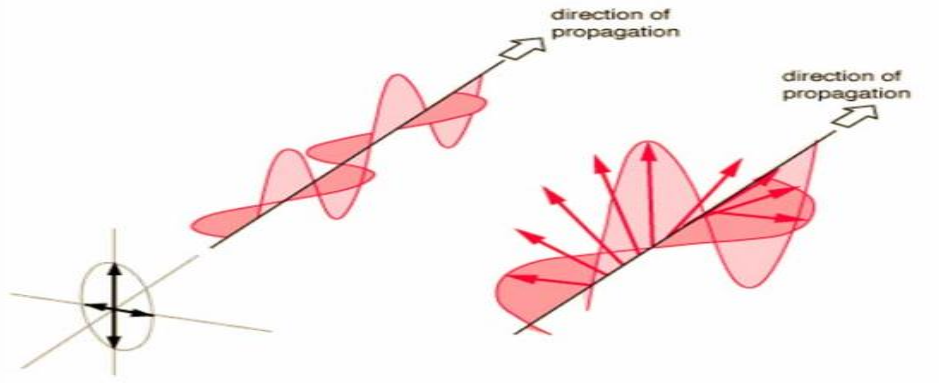

Figure 2.6: Elliptical Polarization (Picture source: HyperPhysics Website)

2.2 Mathematical Description

For a single photon (Figure 2.2), the electric can be described as the sum of its $\hat{x}$ and ŷ components by using the conventional wave equation solution as follows,

$$\vec{E}(z,t) = \vec{E}_x(z,t) + \vec{E}_y(z,t) \quad (2.1)$$

Where:

$$\vec{E}_x(z,t) = \vec{E}_{0x}(z,t)\, cos\,(kz - \omega t) \quad (2.2)$$
$$\vec{E}_y(z,t) = \vec{E}_{0y}(z,t)\, cos\,(kz - \omega t + \epsilon) \quad (2.3)$$

E_{ox}: Electric field amplitude of the $\hat{x}$ component.

E_{oy}: Electric field amplitude of the ŷ component.

k: wave number -$2\pi/\lambda$

ω: frequency -c/λ

ϵ: phase shift between the $\hat{x}$ and ŷ component.

Stemming from these equations, any polarization state can be produced with the proper choice of the electric field amplitudes E_{ox} and E_{oy} and the phase difference (ϵ) between them. There are special cases of amplitude and phase that are very important. These are:

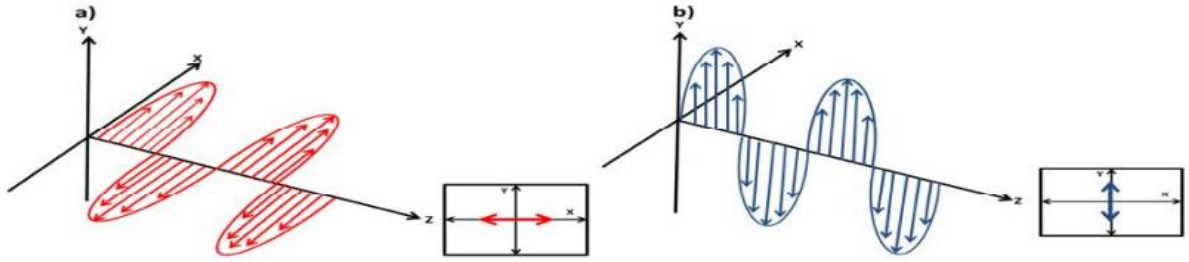

Figure 2.7: (a) Linear Horizontal Polarization (LHP), if E_{ox}=0. (b) Linear Vertical Polarization, if E_{oy}=0 irrespective of their phase difference.

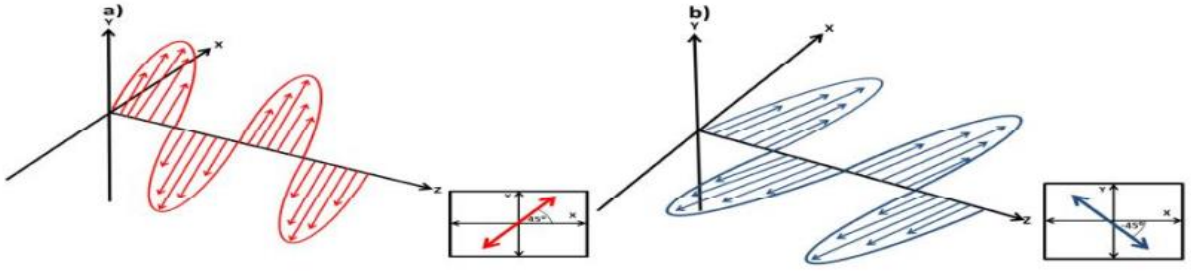

Figure 2.8: (a) Linearly +45^{o} polarized light. (b) Linearly -45^{o} polarized light

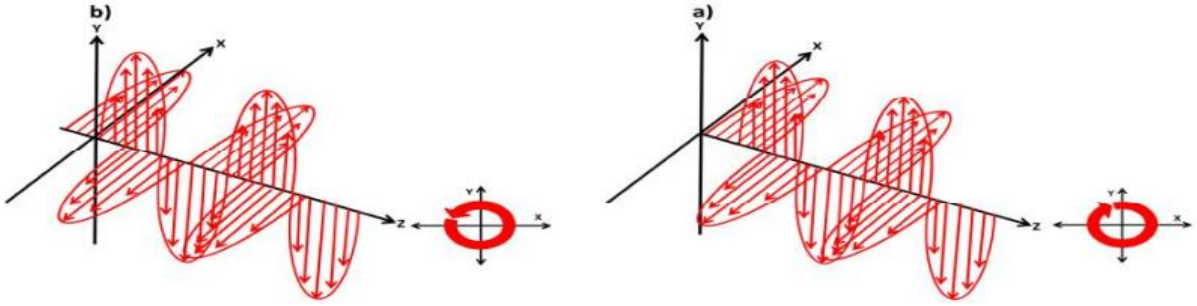

Figure 2.9: (a) Circular right-hand polarization representation, where $\Delta=\pi/2$. (b) Circular left-hand circular polarization representation, where $\Delta=-\pi/2$.

2.2.1 Stokes Parameters

The mathematical description in the previous section (Eq. 2.1-2.3) helps to determine the polarization state of a single photon. In order to measure the energy of the polarized light, *Sir Gorge Stokes (1852)* introduced two or more photons with each unique polarization state and described polarization of light. The state of polarization and their sum is described by the Stoke vectors in which the components are the four Stokes parameters;

$$s_0^2 = s_1^2 + s_2^2 + s_3^2 \qquad (2.4)$$

Where:

$$
\begin{aligned}
S_0 &= E_{ox}^2 + E_{oy}^2 \\
S_1 &= E_{ox}^2 - E_{oy}^2 \\
S_2 &= 2E_{ox}E_{oy}\cos(\delta y - \delta x) \\
S_3 &= 2E_{ox}E_{oy}\sin(\delta y - \delta x)
\end{aligned}
\tag{2.5}
$$

The Stokes parameters S_0, S_1, S_2, S_3 allow simple computation of the new polarization state and the ability to describe the polarization state of partially polarized light which makes the technique unique. practically, the Stokes parameters can be measured by using polarizer (for filtering) and resulting intensities are compared as follows,

$$
\begin{aligned}
S_0 &= i_{0^\circ} + i_{90^\circ} \\
S_2 &= i_{0^\circ} - i_{90^\circ} \\
S_3 &= i_{+45^\circ} - i_{-45^\circ} \\
S_4 &= i_{RH} + i_{LH}
\end{aligned}
\tag{2.6}
$$

Where i_{0° indicates the light intensity passing through a polarizer oriented at 0°, i_{90° is the light intensity passed through a polarizer oriented at 90° etc. i_{RH} and i_{LH} depicts the amount of light with circular polarization that is right hand and left hand oriented. Categorically, the Stokes parameters can be calculated if the parameters of (Eq. 2.6) are measured directly using their definitions:

$S =$

$S_0 \rightarrow$ total intensity.

$S_1 \rightarrow$ preponderance of “horizontal” polarization states over “vertical” states.

$S_2 \rightarrow$preponderance of the $+45^o$ states over -45^o states.

$S_3 \rightarrow$preponderance of the right circular vs left circular states.

With the Stokes parameters, we can possibly directly determine the degree of polarization (DoP) of any optical signal through its *S* components. Basically, the DoP estimates the Fraction of the optical signal that is polarized. The DoP of the completely polarized signal is equal to the unit, while the DoP of the unpolarized optical signal is zero, given by Equation (2.7).

If a light beam is linearly polarized, the elliptical and circular polarizations are zero. Therefore, its DoP is generally known as the degree of linear polarization (DoLP). The degree of linear polarization of a beam of light is illustrated by Equation (2.8).

To obtain all optical properties of partially polarized light, these three parameters are essential to know: the wave intensity, angle of polarization (AoP) and degree of linear polarization (DoLP). The angle of polarization (AoP) can be described by Equation (2.9).

$$\text{DoP} = \sqrt{(S_1^2 + S_2^2 + S_3^2)}\,/S_0 \tag{2.7}$$

$$\text{DoLP} = \sqrt{(S_1^2 + S_2^2)}\,/S_0 \tag{2.8}$$

$$\text{AoP} = (1/2) \cdot \arctan\,(S_2 / S_1) \tag{2.9}$$

2.2.1.1 Stokes Representation of Polarized Light

This section explains the usage of Stokes parameters for the representation of polarized light which are Unpolarized light, partially polarized light and completely polarized light.

2.2.1.1.1 Unpolarized Light

A light is referred to as unpolarized light if the vibration of light is more than one plane. This means that the vibration of light particles is scattered. This could come from a light source emitted by the sun, a candle flame or a lamp in a room. Such light waves are created by electric charges that oscillate in all directions and paths. In relation to the Stokes vector,

the mean value of the last three Stokes parameters, S_1, S_2 and S_3 are zero and the degree of polarization is zero.

$$S_{unpolarized} = S_0 \begin{bmatrix} 1 \\ 0 \\ 0 \\ 0 \end{bmatrix} \tag{2.10}$$

2.2.1.1.2 Completely Polarized Light

A fully polarized light can either be Linearly, circularly or elliptically polarized. A light is said to be plane or linearly polarized if all the electric field vectors vibrate in the same plane, parallel to a fixed direction. A fully polarized light can be described by using ellipticity χ, orientation ψ and Stokes vector as illustrated below:

$$\begin{pmatrix} S_0 \\ S_1 \\ S_2 \\ S_3 \end{pmatrix} = \begin{pmatrix} S_0 \\ S_0 \cos 2\chi cos2\psi \\ S_0 \, sin2\chi cos2\psi \\ S_0 \, sin2\chi \end{pmatrix} \tag{2.11}$$

Regarding the Stokes vector approach for a fully polarized light, only three of the Stokes vectors are independent, since $S_0 = \sqrt{(S_1^2 + S_2^2 + S_3^2)}$. The last three elements of the Stokes vector depict the cartesian coordinates of the part of the wave that is polarized.

2.2.1.1.3 Partially Polarized Light

Partially polarized light wave is an electromagnetic wave that consists of the mixture of completely polarized light and unpolarized light, thus it is not fully polarized. Partially polarized light occurs if the electric field vectors have a preferred direction of oscillation.

$$I = I_{pol} + I_{un}$$

Stokes vectors are used to describe partial polarization of light beams as the light progresses through an optical system. The Stokes vector approach for a partially polarized light, the total power is greater than the fully polarized component. It can be expressed as:

$$s_0^2 \geq s_1^2 + s_2^2 + s_3^2$$

We may introduce degree of polarization (ρ) as a measure for partially polarized light as:

$$\rho = \frac{I_{pol}}{I_{tot}} = \frac{\sqrt{S_1^2 + S_2^2 + S_3^2}}{S_0} \leq 1 \text{ or } \frac{I_{\parallel} - I_{\perp}}{I_{\parallel} + I_{\perp}} \quad (2.12)$$

Where I_{pol} represent the polarized intensity and I_{tot} is the total intensity, $I_{\parallel}$ and $I_{\perp}$ are the intensity parallel and perpendicular to the surface plane. The degree of polarization (ρ) takes value in between 0 and 1. However, if the light beam is totally unpolarized, that is $I_{pol} = 0$, then the degree of polarization (DoP) is 0 and if the light beam is totally polarized as such $I_{un} = 0$, the degree of polarization (DoP) is one. A Stokes vector with degree of polarization between 0 and 1 characterizes a partially polarized beam. To determine the parameters of the ellipse of the polarized component, the parameters of the Stokes vector can be expressed in different forms as such:

$$\begin{pmatrix} S_0 \\ S_1 \\ S_2 \\ S_3 \end{pmatrix} = \begin{pmatrix} I_{tot} \\ I_{pol} \cos 2\varphi \\ I_{pol}\, sin2\varphi cos\delta \\ I_{pol}\, sin2\varphi sin\delta \end{pmatrix} \quad (2.13)$$

Where φ is the angle of polarization and δ is the polarization phase.

2.2.2 Mueller Matrices

Generally, the polarization ellipse is a non-standard form. The polarization state (polarization ellipse) can be changed by changing the amplitude (**S)**, the phase or rotating the ellipse. A polarized beam with a given polarization state transverse through polarization elements in which the beam obtains a new polarization state. This process is illustrated in the following figure below:

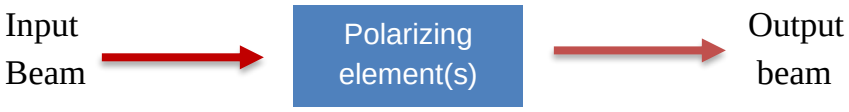

Figure 2.10: polarization process.

The input beam is described by Stokes vector S, and the output beam is characterized by S′. This depicts that we can model the change of polarization state as a function **s′ = F(s),** where F is a sequence of transformations that change the input beam polarization state S to a new state S′. It is of the assumption that the S and S′ are linearly related that can be written as a 4 × 4 transformation matrix known as the **Mueller Matrix [16].** The change of polarization can be model as follows:

$$\begin{bmatrix} S_0' \\ S_1' \\ S_2' \\ S_3' \end{bmatrix} = \begin{bmatrix} m_{00} & m_{01} & m_{02} & m_{03} \\ m_{10} & m_{11} & m_{12} & m_{13} \\ m_{20} & m_{21} & m_{22} & m_{23} \\ m_{30} & m_{31} & m_{32} & m_{33} \end{bmatrix} \begin{bmatrix} S_0 \\ S_1 \\ S_2 \\ S_3 \end{bmatrix} \tag{2.14}$$

All the elements in the 4 × 4 Mueller Matrix are real quantities. The matrix above can be written as a matrix equation:

$$\mathbf{S' = M \cdot S} \tag{2.15}$$

2.2.2.1 Measuring Polarization State

From the equation (2.14), the Stokes parameters of incident light can now be measured by using a rotated linear polarizer and a phase retarder **[17].** The rotating linear polarizer is composed of a linear polarizer and optic rotator. The linear polarizer permits the light to align with a certain direction to propagate through it and absorbs the rest. The optic rotator on the other hand allows the light to transmit through it and rotates the polarization ellipse. The Mueller Matrix of rotated linear polarizer with an angle (α) and with transmission coefficient (τ) is:

$$M_{pol}(\alpha) = \frac{\tau}{2}\begin{bmatrix} 1 & cos2\alpha & sin2\alpha & 0 \\ cos2\alpha & cos^2 2\alpha & cos2\alpha\ sin2\alpha & 0 \\ sin2\alpha & cos2\alpha\ sin2\alpha & sin^2 2\alpha & 0 \\ 0 & 0 & 0 & 0 \end{bmatrix} \quad (2.16)$$

From this equation, the Mueller Matrix of a linear polarizer for horizon, vertical, 45°, and circular polarizer can be computed.

Concretely, phase retarder as a polarization element changes the phase of the optical beam. It can also be called a phase shifter. A phase retarder has a fast axis normally along the *x* axis and slow axis along the y axis. The light transmitted through a retarder will shift phase between the orthogonal components. The Mueller Matrix for a retarder fast axis at angle θ and shift phase by δ can be written as:

$$M_{pol}(\theta,\delta) = \begin{bmatrix} 1 & 0 & 0 & 0 \\ 0 & cos^2 2\theta + sin^2 2\theta cos\delta & (1-cos\delta)\, sin2\theta\, cos2\theta & -sin2\theta sin\delta \\ 0 & (1-cos\delta)\, sin2\theta\, cos2\theta & sin^2 2\theta + cos^2 2\theta cos\delta & cos2\theta sin\delta \\ 0 & sin2\theta sin\delta & -cos2\theta sin\delta & cos\delta \end{bmatrix} \quad (2.17)$$

2.3 Polarization Reflectance Model

On a daily basis we encounter polarized light even if the Sun produces light with a very small degree of polarization. Unpolarized light ray changes polarization state when it interacts with a surface and it can become highly polarized in the direction parallel to the surface. Polarization depends on the surface the reflection occurs and upon the angle of angle of the incident light approaching the surface. Reflection on non-metallic surfaces such as water, plastics, a road with asphalt etc. reflects light such that there is high concentration of vibration. The reflected light will be linearly polarized in the direction parallel to the surface. There is a specific incident angle where the reflected angle meets this condition, that angle is known as **Brewster angle** and it's given by:

$$\tan \theta_B = \frac{n_2}{n_1} \tag{2.18}$$

The expression can be derived using Snell's polarization law of reflection. The illustration in Figure (2.11) describes the geometry. The Brewster law can be generated by using **Snell's Law [18]:**

$$\theta_i = \theta_r \tag{2.19}$$
$$n_1 \sin \theta_i = n_2 \cos \theta_t$$

The smell's law gives the relation of the indices of refraction (n) of the two mediums of the direction of propagation in terms of angles to the normal.
Then the Brewster angle is:

$$\frac{\sin \theta_i}{\cos \theta_t} = \frac{n_2}{n_1} \Rightarrow tan\theta_B = \frac{n_2}{n_1} \tag{2.20}$$

A reflected light from an unpolarized incident light is said to be polarized perpendicular to the incident plane or parallel to the surface if the angle is at Brewster's angle.

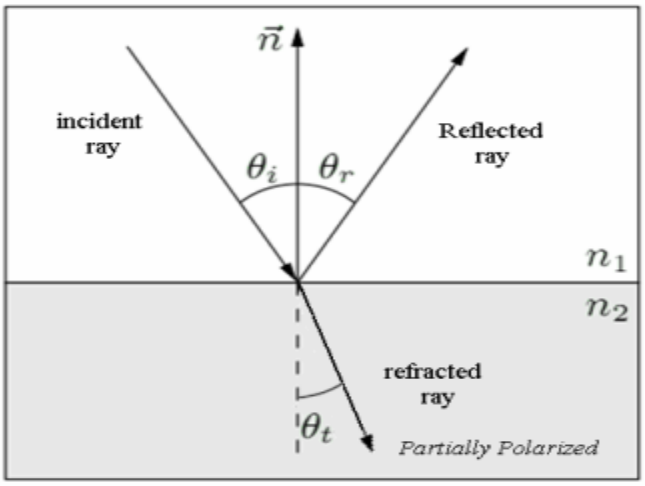

Figure 2.11: Snell's Law illustration of Polarization by Reflection.

2.3.1 Fresnel Coefficient

The Fresnel equation expresses the reflection and transmission of electromagnetic waves at an interface. It describes the reflection and transmission of incident waves parallel and perpendicular to the incident plane. Considering a dielectric surface where Snell's law can give the relation between the incident and transmitted angle, Fresnel's equation can be described in terms of the angle of incidence and transmission.

Fresnel equation gives the reflection coefficient as:

$$r_{\parallel} = \frac{\tan(\theta_i - \theta_t)}{\tan(\theta_i + \theta_t)}$$
$$r_{\perp} = -\frac{\sin(\theta_i - \theta_t)}{\sin(\theta_i + \theta_t)} \quad (2.21)$$

The transmission coefficients are given as:

$$t_{\parallel} = \frac{2\sin\theta_t cos\,\theta_i}{\sin(\theta_i+\theta_t)\cos(\theta_i-\theta_t)}$$
$$t_{\perp} = \frac{2\sin\theta_t cos\,\theta_i}{\sin(\theta_i+\theta_t)} \quad (2.22)$$

In addition, it should be noted that the amplitudes of these coefficients are fractional amplitudes and to get the fraction intensities for reflection and transmission, it must be squared.

2.4 Polarization Imaging

The polarization imaging allows the study of the polarization state of a light wave. This technique enables reconstructing 3D shape on an object as a result of the reflection or refraction study of an unpolarized light wave, which is called “Shape from Polarization”. Polarization imaging can be used to distinguish dielectrics and metallics in industrial vision **[19]**.

2.4.1 Principle

In the case of partially linearly polarized light, an unpolarized light wave becomes partially linearly polarized after being reflected on a surface, depending on the surface normal and the refractive index of the media it acts on. The polarization state of a partially linearly polarized light wave can be studied according to Wolff **[20],** considering it as a sum of two components: a completely unpolarized light wave and a completely linearly polarized light wave. Consequently, the polarization sensor has to be able to compute the following parameters:

I. Light magnitude ***I*,**
II. Degree of polarization $\boldsymbol{\rho}$**,**
III. Angle of polarization $\boldsymbol{\varphi}$**.**

The degree of polarization is the relative proportion of the polarization component which varies from 0 from a completely unpolarized light to 1 corresponding to completely linearly polarized light.

2.4.2 Polarization Imaging using Rotating Polarizer

To determine the polarization state of the partially polarized light, a rotating linear polarizer is set up in front of the camera. The relationship of the between the magnitude of light I_p transmitting a partially linearly polarized light through a rotating polarizer and the angle α of polarizer filter is:

$$I_p\,(\alpha) = \frac{I_{max} + I_{min}}{2} + \frac{I_{max} - I_{min}}{2}\, cos\,(2\alpha - 2\varphi), \tag{2.23}$$

Where $\boldsymbol{I_{max}}$ and $\boldsymbol{I_{min}}$ are the minimum and maximum polarization intensity seen through the polarizer and φ is the angle of polarization. The equation can be written in the form:

$$I_p\,(\alpha) = \frac{I_{tot}}{2}\,(1 + \rho\, cos\,(2\alpha - 2\varphi). \tag{2.24}$$

From the equation, the magnitude of light I and the degree of polarization ρ (proportion of the polarized component) can be derived as:

$$I = I_{max} + I_{min}\,,\;\; \rho = \frac{I_{max} - I_{min}}{I_{max} + I_{min}}, \tag{2.25}$$

The angle of the linearly polarized component $\boldsymbol{\alpha}$ is given by the phase shift of the sinusoid.

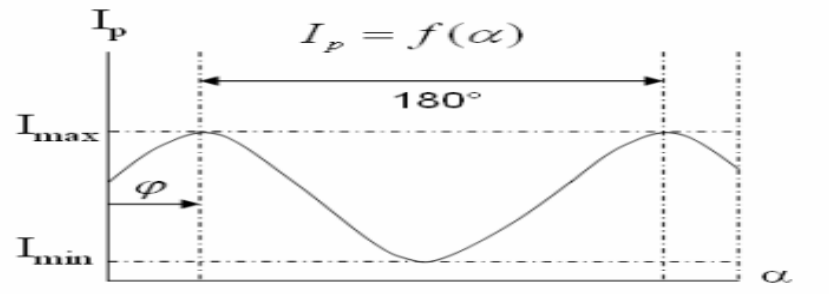

Figure 2.12: variation of intensity I_p of angle of polarizer α.

The motive of the principle of polarization imaging is to compute the three parameters I, ρ and α. In order to calculate these parameters, a minimum of three images must be observed corresponding to three orientations of the polarizing filter **[21]**, such as I_0, I_{45}, and I_{90}. For this method, the images can be computed in real time but it is very sensitive to noise.

2.5 Polarization Camera Operations

2.5.1 SALSA Camara

The Bossa Nova Technology SALSA camera has the capability for both polarization analysis and regular digital camera. The main feature of the Salsa camera is the ability to show/display full stokes parameters and also calculation in real time for each pixel of an image. SALSA can operate in active and passive imaging and the application ranges from target detection, 3D reconstruction and Robotic vision.

Figure 2.13: SALSA Camera

SALSA camera captures raw images sequentially and carryout live measurement of the full stokes vector for each pixel of the images at video rate. The software then calculates the polarization state of the light and polarization parameters can be visualized as such stokes parameters (S_0, S_1, S_2, S_3), Degree of Polarization and Angle of Polarization or Ellipticity angle in real time (see Figure 2.14).

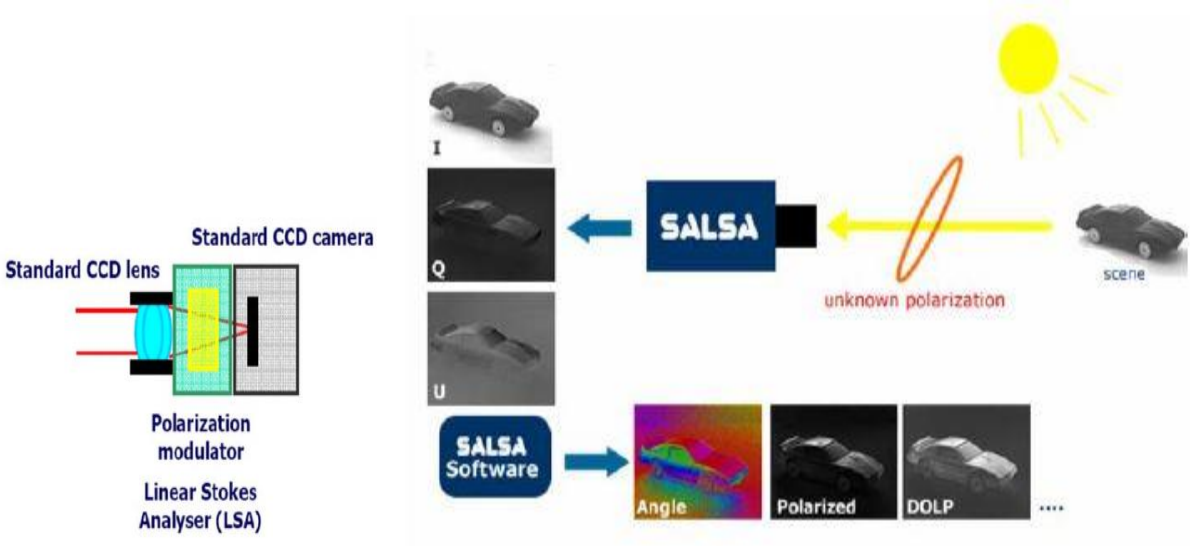

Figure 2.14: SALSA Camera Mechanism and work principle

[Image source: SALSA Bossanovatech 2010].

The SALSA camera uses a distinct polarization filter subjected to ferroelectric liquid crystal which decreases the time for the acquisition of the images. The camera size is 3.2"x3.2"x4" (80mm x 80mm x 100mm) and it has an 8 or 12-bit CCD standard lens, one megapixel, and C-mount lens that is interchangeable. The camera calibration is factory calibrated.

2.5.2 Equinox Polarimetric Camera

The equinox multispectral camera is a 3CCD polarimetric camera, each one receiving filtered green, blue or red color ranges. The multispectral polarimetric camera can do measurement of 3 out of 4 stokes parameters such as the intensity, the angle of polarization i.e., the orientation of the linearly polarized light and degree of linear partial polarization. The camera system has three channels with 1024×1024 resolution, 12-bit dynamic range and capable of real time polarimetric video. The system is relying on an optical beam splitter that allows modular multispectral or polarimetric configuration, Figure (2.15) shows the camera and illustrates examples of captured images by this camera.

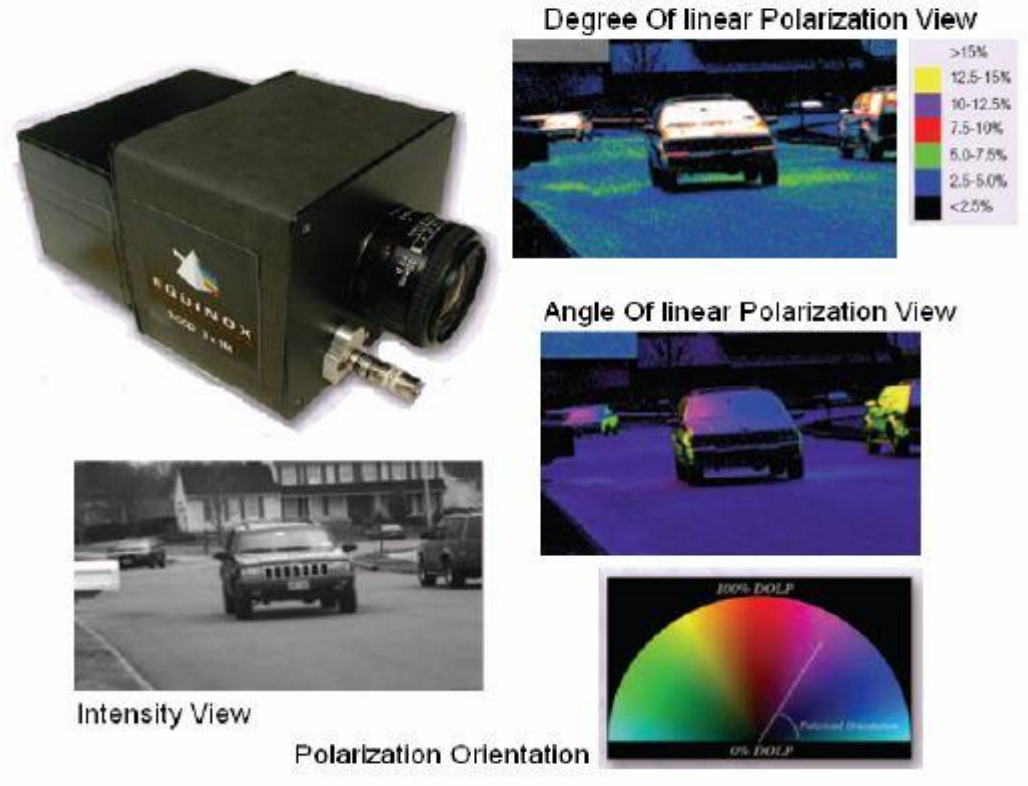

Figure 2.15: showing Equinox 3CCD Polarimetric Camera, processing of the camera with illustration of captured images [Image source: Equinox 2010]

2.5.3 FLUXDATA Camera

The Fluxdata FD-1665P 3 CCD Camera has the capability to capture images and video at three linear polarization directions simultaneously without delay in time with full color. This Fluxdata camera has been used for separation of specular from diffuse reflectance for material analysis, to identify man-made objects in natural surroundings and to detect stress in aircraft gathering.

Figure 2.16: Fluxdata Camera

The Fluxdata camera addresses all the above-mentioned areas, capturing concurrently registered video from its three sensors. The configuration requires user-specified filters in front of each sensor. The camera has three CCD sensors on three polarizers (see Figure 2.17)**.** The camera uses a 3-ways beam splitter prism with two coating surfaces and this splits the incoming light into three components with equal spectral components. The Fluxdata camera polarization filters are oriented at 0, 45 and 90 degrees and the camera can either be configure with color or monochrome sensors for each channel.

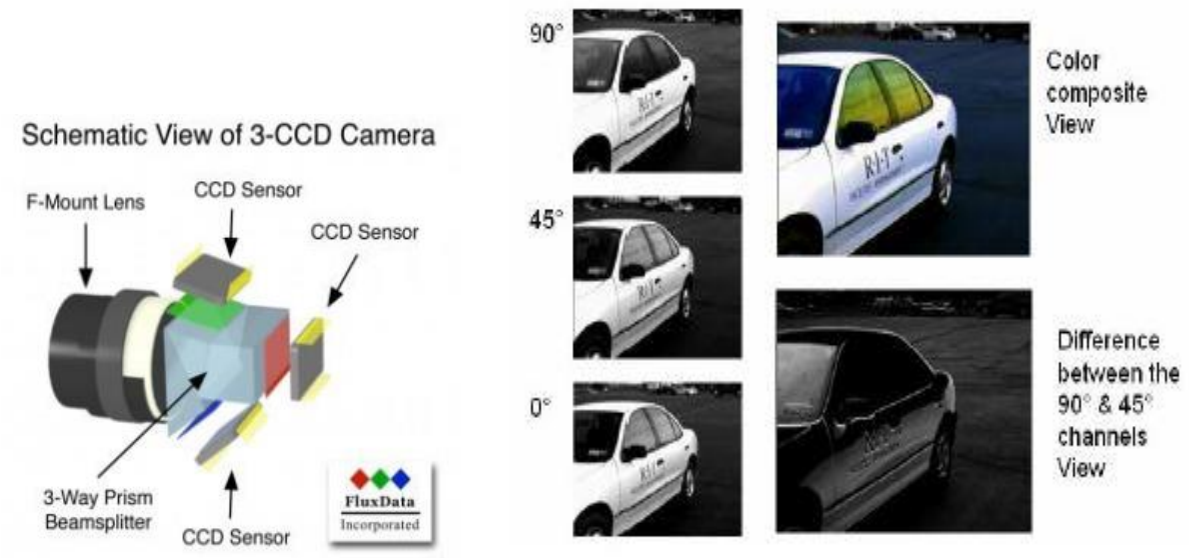

Figure 2.17: Fluxdata Color CCD sensors and illustration of captured images from the camera [Image source: Fluxdata 2009]

The camera sensor is a progressive scan charge coupled divide (CDD) Sony ICX285 with the size of the sensor of 1628×1236 pixels. The camera is capable of 30 frames per second at full resolution. For digital images, the CCD sensor converts light into electric charges that process to electric signals. The sensor is dependent on photoelectric effect to form an electric signal from the captured incoming light. It offers 1.4 megapixels and an F mount lens that is interchangeable and the camera size is (4.6"x3.5"x4.4").

2.5.4 phoenix Polarization Camera

The Phoenix polarization camera is a new generation polarimetric camera which offers high quality polarized imaging. The camera features Sony's IMX250MZR CMOS polarized sensor. This sensor is a 5MP global shutter sensor, built upon IMX250 Sony Preguis CMOS mono sensor which incorporates a layer of polarizing filters above the photodiodes. The array layer of the polarizer is placed on-chip and it is an air-gap nano wire grid covered with an anti-reflection material which surprises flashes, noise and ghosting.

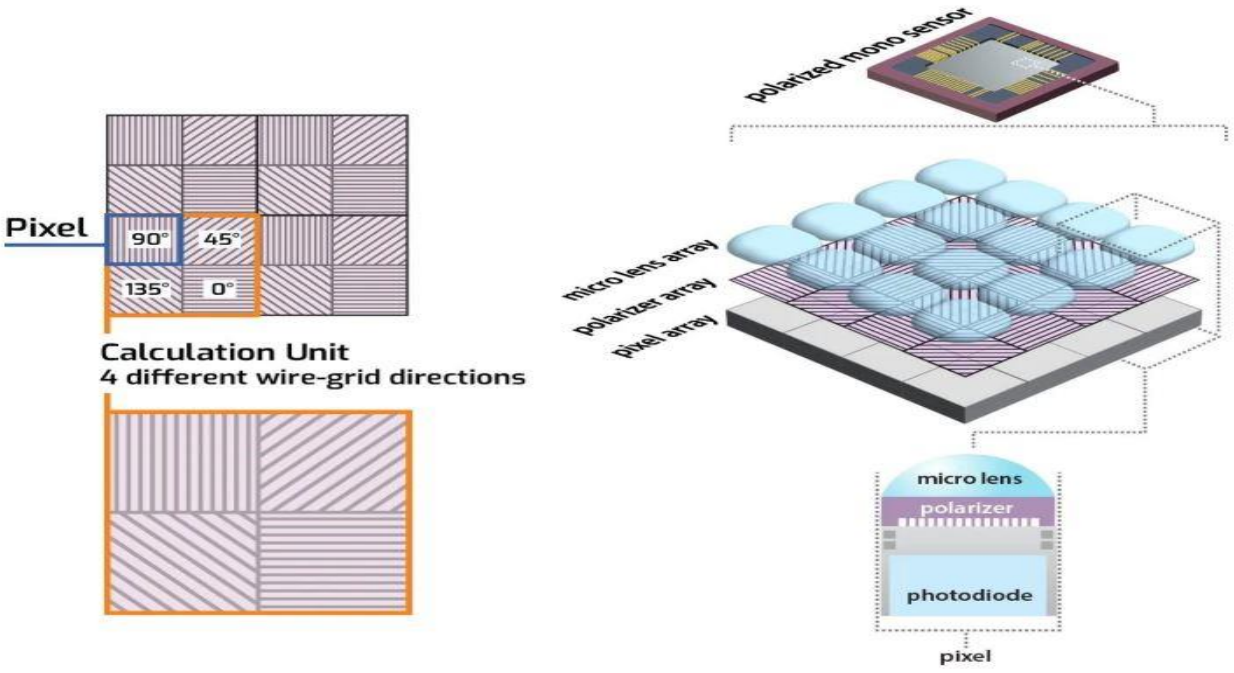

Figure 2.18: Phoenix Sony's polarens 4-pixel block polarizer design

[Image source: Lucid Vision Labs]

The sensor comprises of four different angle polarizing filters ($0^{\circ}, 90^{\circ}, 45^{\circ}$, and 135°) which are placed on each pixel, allowing very accurate alignment with the pixel array. Every block of the Sony's IMX250MZR four pixels makes up a calculation unit which allows for the detection of all linear angles of polarized light. Basically, the relationship between these innovative 4 pixels directional polarizer block design allows the estimation of both the direction and degree of polarization.

2.6 Application of Polarization Imaging

Application of Polarization have been long used in Machine or computer vision for object detection, contrast enhancement, reduction of glare from transparent object and for automation in the robotics field to increase the visibility of image i.e., object analysis or to aid navigation. This section explains some general typical setup operation of polarization application.

Glare Reduction

Light reflection on objects can sometimes make it difficult for surface inspection of the object. In advance image analysis, glare is a common challenge when the product is being imaged. Polarization is very effective for glare reduction and producing perfect image of the object. For instance, when light is reflected off a horizontal surface, the resulting glare is polarized and the light filtered at the correct state of polarization enables the reduction of such glare with minimal impact on the rest of the image. The image below illustrates a polarized reflected light reducing reflection and glare from the original (unpolarized reflected) image:

Figure 2.19: Glare reduction [Image source: Lucid Vision Labs]

Improving Contrast

In polarization imaging, contrast can be improved in low light situations by detecting the angle of polarization off objects. That is, in a low-contrast environment with several dark objects, it can be hard to differentiate the object shapes and boundaries. polarization technique improves contrast (see Figure 2.20) and show the object more accurately in which makes it possible to identify the boarders and forms of the object.

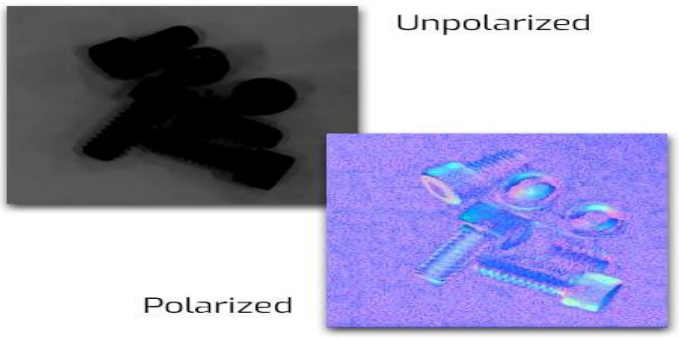

Figure 2.20: Image Contrast enhancement [Image source : Lucid Vision Labs]

Object Detection

There are so many cases or scenarios whereby distinguishing objects from their environment can be difficult. Using polarized imaging, it can detect objects by locating the unique angle of the reflected light from the object on that scene. An example is shown below:

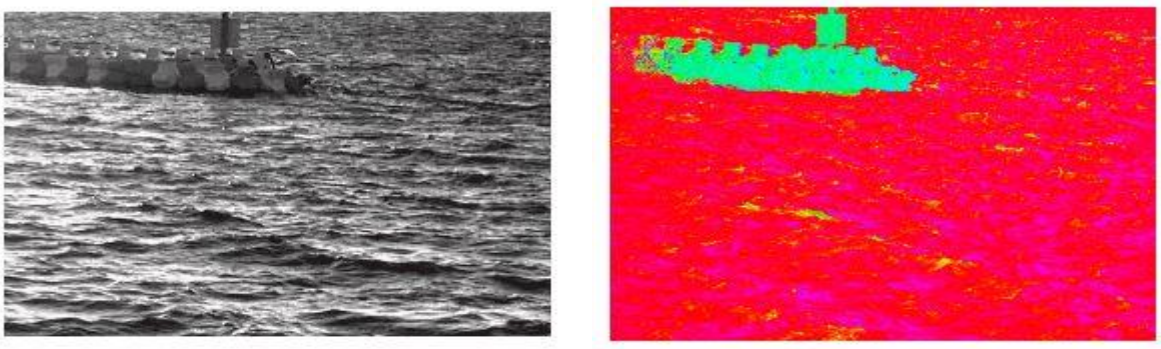

Figure 2.21: Object detection using polarization imaging [Image source: Lucid Vision Labs]

2.7 Shape Estimation and Reconstruction

This section discusses different methods for shape estimation and reconstruction of objects in the area of research where people carry out different research.

2.7.1 Shape from Polarization

There are various factors that affected polarization in a scene, such as surface materials, surface curvature, surface shape and objects position in respect to light source, and polarization can therefore provide useful information about those objects **[22]**.

Shape from polarization (*sfp*) is a technique that estimates surface normals by analyzing the polarization properties of reflected light. Shape from polarization is an application regarded as more general techniques of polarization imaging **[20]** that offers the possibility linking polarimetric parameters to depth in the observed scene. Shape from polarization aims at measuring the normal at each point of the surface observed by measuring the polarization state of the first reflection. The major issue with shape from polarization is angle ambiguity. Miyazaki *et al* **[23]** applied the technique for transparent objects and use polarization analysis to resolve two ambiguities of the reconstruction of the transparent objects. This method used two different views to obtain two sets of data of polarization, the observation of the object was done twice from the same camera rotating the object at small angle and several external illumination light sources from all direction producing specular reflection all over the surface of the object. The unique surface orientation can be determined by the degree of polarization at the corresponding point of each set of polarization data.

Morel *et al* **[24]** applied this technique for metallic object using Fresnel reflectance model with complex index of refraction. This method is stretched to metallic surfaces since their refractive indexes are complex in because the degree of polarization from Fresnel reflection method cannot be directly applied to the surfaces. He resolved the ambiguity about the

determination of azimuth angle ∅ from the angle of polarization φ by varying the illumination with an active lighting system (see Figure 2.22). the ring LED is divided into four parts which can be independently electrically controlled.

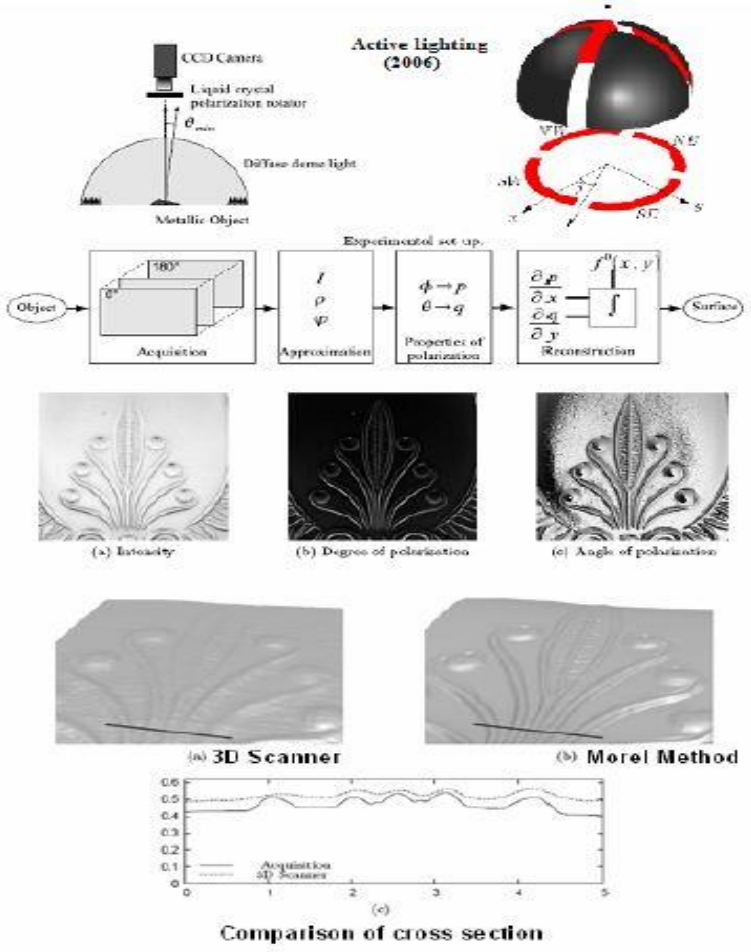

Figure 2.22: Smooth metallic object shape reconstruction; experimental object and result compared with 3D Scanner [Morel et al. 2005] and additional active lighting resolving the problem of ambiguity [Morel et al. 2006]

However, shape can also be estimated from dielectric objects by using the cues from diffuse polarized reflections. Atkinson and Hancock **[25]** combined a polarization and shading information system for 3D reconstruction from two views of dielectric surfaces. The polarized images are captured by using a linear polarizer mounted in front of CCD camera, in which the diffuse reflected images processes to estimate the surface normal using Fresnel

theory. The ideology behind Atkinson method is to combine shading information to improve the surface normal by doing measurement of statistics on pixel brightness prior to the surface orientation.

Ferraton proposed a method **[26]** using multispectral measurement which can be used to solve of 3D measurement ambiguities by polarization imaging during the process of measurement. The method comprises of a CCD camera, a polarization rotator, and a diffuse dome light with three wavelengths. With this system as illustrated in Figure (2.23), the 3D surfaces are automatically estimated in few seconds.

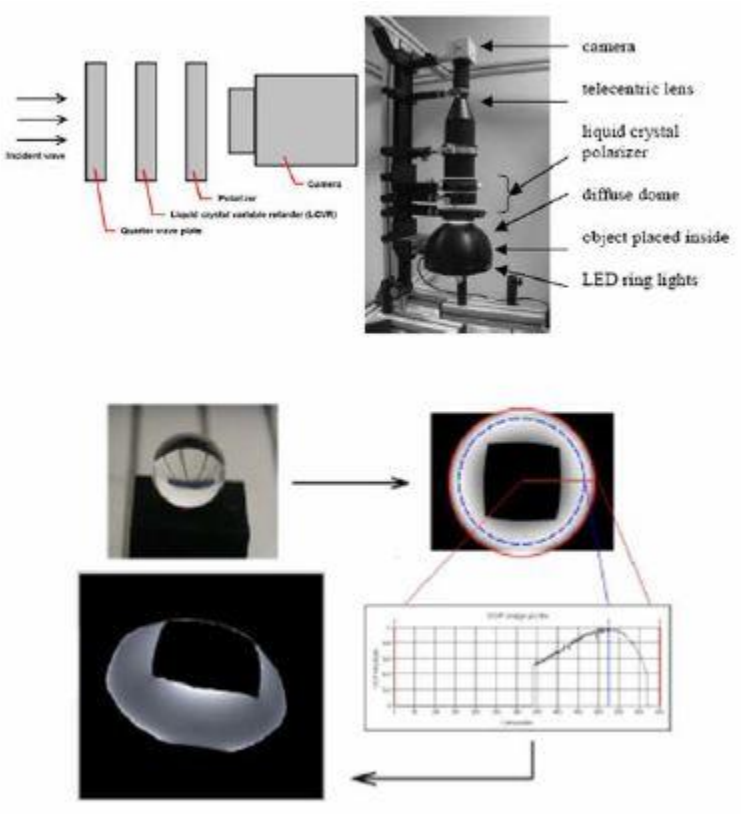

Figure 2.23: Experiment, optical design and shape from polarization result of transparent object [Ferraton et al. (2008)]

2.7.2 Shape from Shading

Shape from shading have been an extensive research for the past few decades. In the early 1970s, Horn **[27]** and Krakauer **[28]** introduced Shape from Shading (SFS) to computer vision. The conventional approach to SFS is to estimate a mapping between pixel intensity measured and the surface orientation at each point. This prompts several areas to be addressed.

One of the several questions raised was, how can one determine the relationship between the surface orientation and the pixel brightness? The majority of SFS algorithms assume that surface reflectance is Lambertian **[29]**. This simply insinuates that the reflecting intensity is determined only by the ratio of the reflected incident light at the normal incidence (albedo) and the proportion to the cosine of the zenith angle. This simply implies that an image should be dependent on the direction of illumination. Worthington and Hanock **[30]**, established a SFS algorithm for Lambertian surfaces in which the pixel brightness was assumed as hard constraints on the surface normal. Worthington **[31]** later explained how albedo changes can be integrated into the technique.

For a long time, it has been known that the Lambertian assumption has been hardly accepted **[32]**. Ragheb and Hancock **[33]** tried to conquer this problem by making use of some of the theoretical reflectance models to correct images by making them appear as Lambertian. Dupuis and Oliensis **[29]** developed an algorithm that directly calculates depth by moving away from the image brightness point in order to avoid the challenges with calculating a global needle map altogether.

Another promoted question was, can the two degrees of freedom of a surface orientation be estimated from a single intensity measurement? Prior to this, one must either use multi-view or make constraints about the surface geometry to conquer the under-constrained nature of SFS. Ikeuchi and Horn **[34]** impose the constraints that:

1. The surface reconstructed must produce the same brightness as the image intensity.
2. The surface is continuous and smooth.

Brooks and Horn **[35]** later adopted these constraints. Shimishon, Moses and Lindenbaum **[36]** developed an algorithm specially constrained for symmetric objects. This basically overcomes the challenges that SFS is under-constrained and promising results has been shown for face recognition. Prior to Frankot and Challappa **[37]** seminar paper, the smoothness constraint is introduced by using integration. This implies that the initial set of surface gradient estimates were mapped upon the closest set so that Schwartz's theorem can be applied. The relevance of this paper is because surface orientations (normal) and a global integration method is generated for recovering of the depth. However, any method designed to recover a needle map, the Frankot-Chellappa method can be used for converting it to depth. This method can be perfectly applied to a field of smooth surface normal.

In recent work, Agrawal, Chellappa and Raskar **[38]** made a proposition of a related global method that can be used for recovering depth from needle maps by solving linear system equations. This method is a non-iterative technique that avoids any error propagation and doesn't depend on a choice of basic functions unlike the earlier Frankot-Chellappa method. Simchony, Chellappa and Shao **[39]** presented another technique using integration to obtain a gradient field in order to minimize the error of the least square amidst the original field and the integrable field. Eventually, Robles-Kelly and Hancock **[40]** make use of the changes in surface normal directions to calculate the sectional curvature on the surface.

From the above explanations, it is obvious that SFS is an ill-posed problem. Many researchers have attempted to combine shading with other ideas with the goal to avoid enforcing large geometry constraints. For instance, White and Forsyth **[41]** integrate texture information in a way that a field without ambiguous surface normal can be computed.

2.7.3 Multi-view Stereo Reconstruction

This method is among the most recognized techniques to recover 3D geometry from multiple real-world images **[42]**. The key idea of the multi-view stereo reconstruction is to utilize the fact that 3D points are most likely to be on the surface of a Lambertian object (surfaces with uniform reflectance) if the projection into several cameras gives rise to a consistent color or feature value. Techniques such as graph cut **[43]** or convex relaxation **[44]** can optimize the arising photo consistency-weighted minimal surface problems. In spite of its popularity for real world reconstruction, the method has various well-known shortcomings.

First of all, it is computationally challenging for estimation of dense correspond **[45].** Another limitation is, in the absence of color variations (textureles areas), the consistency assumption of the color degenerates which leads to a reason for regularity or smoothness assumption. The resulting surface problems (photo consistency-weighted minimal) formulation degenerate to Euclidean minimal surface problems shows a shrinking bias which leads to the loss of concavities and other fine-scale geometric details.

2.8 Conclusion

This chapter has described the theoretical background related to polarization of light and explains how to derive polarization reflectance models. Also, the chapter did review of different method involved with shape estimation and reconstruction. The next chapter will explain the methodology carried out to achieve the goal and objectives of the thesis.

Chapter 3

Methodology

This chapter describes the proposed method and implementation for this thesis. The implementation of this thesis was inspired from this paper **[46].** As stated in chapter one, the principal goal of this thesis is to recover shape using polarization properties of the reflected light from a non-Lambertian object. The illustration below shows the overall schematic workflow:

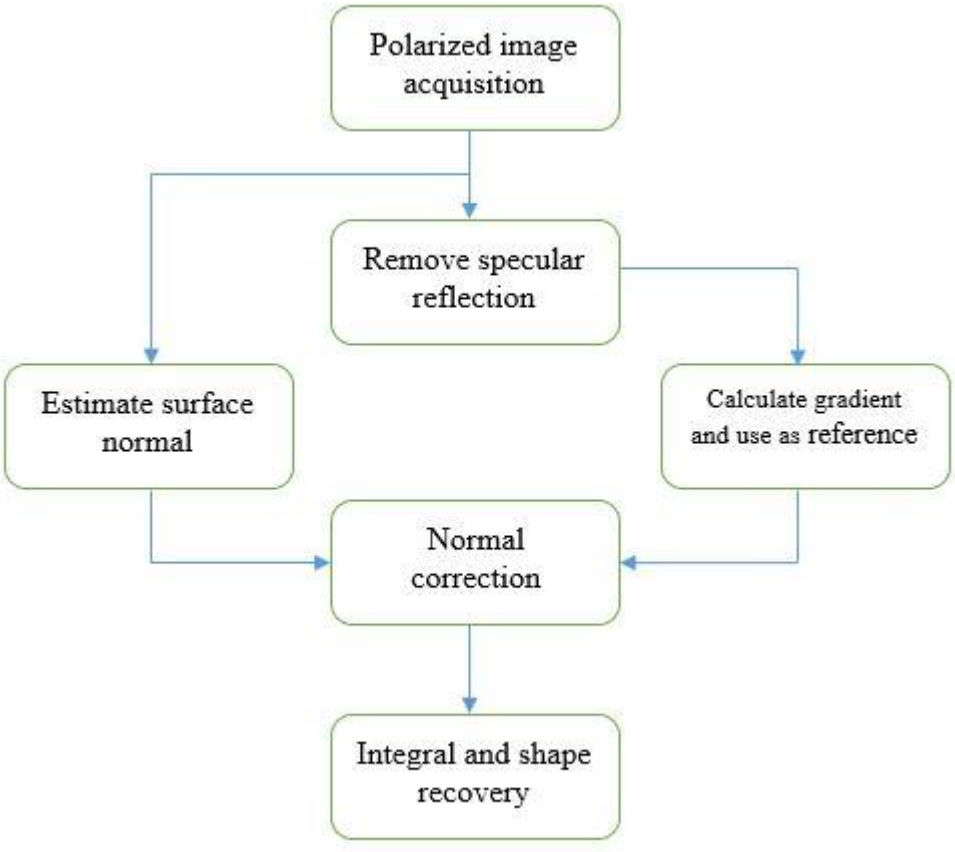

Figure 3.1: overall schematic workflow

3.1 Experimental Setup

The experimental setup shown in Figure (3.2) describes the image acquisition process basically related to the acquisition scene, and the observed images. The polarization detection process was done in an enclosed room (indoor). Specifically, the object used for acquiring the polarization images is a ceramic tea cup with a rough surface under illumination of unpolarized light from a LED light source.

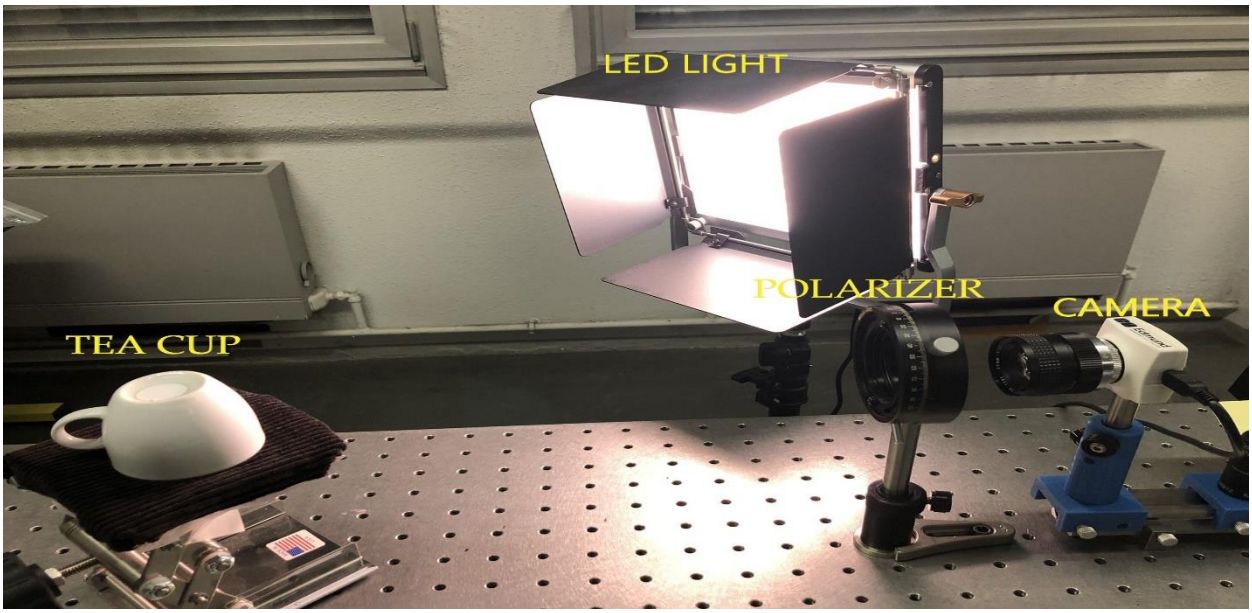

Figure 3.2: The experimental setup

The experiment setup basically shows an unpolarized light source observed through a polarization camera with a rotating polarizer mounted in front of it which allows the acquisition of the polarization images at different orientation of the polarizer. The camera is Edmund optic camera and it's a USB camera with a progressive scan CMOS sensor.

3.1.1 Image Acquisition

Since the surface of the observed image contains the reflection of both diffuse and specular reflection as shown in Figure (3.2), the observed images can be expressed as:

$$I = f_b \cdot I^{sub} \ (sub = diff \ or \ spec), \tag{3.1}$$

Where the superscripts $diff$ and $spec$ depicts diffuse and specular reflection and the coefficient f_b balances the difference in intensity between diffuse and specular reflection. Emerging from Fresnel reflection model **[47-48]**, the specular and diffuse reflection components are said to be partially polarized. Therefore, the observed intensity can be illustrated in equation (3.2), the combination of completely polarized light and unpolarized light.

$$I = I_p^{diff} + I_p^{spec} + I_{np} \tag{3.2}$$

Where I_p^{diff} and I_p^{spec} represents the pure polarized components in diffuse and specular reflection and I_{np} represents the unpolarized components. In this thesis, four (4) polarization images were acquired with a polarizer oriented at different angles such as $0^{\circ}, 45^{\circ}, 90^{\circ}, 135^{\circ}$. Prior to this, equation (3.2) is expanded to (3.3),

$$I_i = f_d(\delta_i)\tilde{I}_p^{diff} + f_s(\delta_i)\tilde{I}_p^{spec} + \tilde{I}_{np}, \ i = 0^{\circ}, 45^{\circ}, 90^{\circ}, 135^{\circ} \tag{3.3}$$

Where the coefficients $f_d(\delta_i)$ and $f_s(\delta_i)$ represents the functions of the orientation δ_i of the polarizer. The I_i is partially linearly polarized reflected light by a surface or natural light contains very little circular polarization components in which can be ignored. The components of the unpolarized $\tilde{I}_{np}$, can then said to be I_{min} by:

$$\tilde{I}_{np} = 2I_{min} = S_0 - \sqrt{S_1^2 + S_2^2} \tag{3.4}$$

Where S_0, S_1, and S_2 represents the elements of the stoke vectors.

Due to the incoherence between each frame, a linear independent function can be built based on I_i and I_{min}:

$$I_D = I_i - I_{min} = A \cdot S$$
$$= [f_d(\delta_i) \quad f_d(\delta_i)] \cdot \begin{bmatrix} \tilde{I}_p^{diff} \\ \tilde{I}_p^{spec} \end{bmatrix} \tag{3.5}$$

Where I_D depicts the difference between the two frames and A represents the modulation of the polarizer to the intensity of the light. For the observation of the image, the orientation of the polarizer where the diffuse is at maximum was set to be 0°, that is $I_0 = I_{max}$. So as the polarized specular and diffuse reflection have different orientation, the modulation function of specular reflection will keep its real formulation.

$$\begin{bmatrix} I_D^1 \\ I_D^2 \\ I_D^3 \\ I_D^4 \end{bmatrix} = \begin{bmatrix} 1 f_s(\delta_0) \\ 1/2\, f_s(\delta_{45}) \\ 0 f_s(\delta_{90}) \\ 1/2\, f_s(\delta_{135}) \end{bmatrix} \cdot \begin{bmatrix} \tilde{I}_p^{diff} \\ \tilde{I}_p^{spec} \end{bmatrix} \tag{3.6}$$

3.2 Separation of Mixed Reflection

According to Wolff's theory **[47],** the reflection of light from a surface emanates from four different phenomena as shown in Figure (3.3). The case 1 depicts specular reflection. Cases 2 and 3 are both considered to be diffuse reflection particularly cases 3 showing major contribution to the diffuse reflection and lastly case 5 shows Diffraction and is negligible. The illustration shows that most surfaces are non-Lambertian with both diffuse and specular reflection.

The general method for separation using only a rotating polarizer is direct and effective. However, it cannot completely separate the diffuse and specular components when the specular incident angle is different from the Brewster angle.

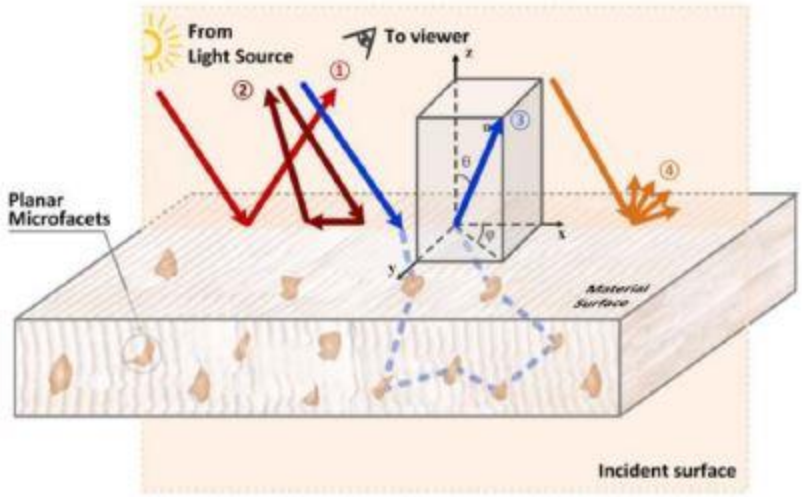

Figure 3.3: Wolff's theory Reflection of light

In this thesis, a separation algorithm is proposed based on probabilistic properties of diffuse and specular components, this algorithm is called Independent Component Analysis (ICA), stemming from *Shinji Umeyama* **[49].** The ICA is a technique that is used for separating mixture signals into their different sources. For instance, when observations of some mixtures of probabilistically independent source signals are made, ICA retrieves the original source signals from the observed mixtures without having prior knowledge of how the sources are mixed. Since both the mixing coefficient and the original signals are unknown, this estimation seems not possible at the first sight but the ICA algorithm accomplishes this by using the probabilistic independence property of the source signals.

However, the ICA compare to the naive septation method can effectively separate the mixed reflectance components even when the angle of incidence is different from the Brewster angle and it does not assume the uniformity of the diffuse reflection. The nonuniform diffuse reflection created by a textured surface may ease the separation since the probabilistic independence between specular and diffuse reflections should be high in this case.

3.2.1 ICA Algorithm for Reflection Component Separation

According to Shinji Umeyama, he made assumption that the images captured through a rotating polarizer can be approximately represented as follows assuming an unpolarized diffuse reflection and a distant light source:

$$I = I_d + f(\varphi)\, I_s, \tag{3.7}$$

He assumed that the observed image I can be separated into two components, the diffuse image I_d and the specular image I_s respectively. That is, the captured image is a linear sum of these images and the specular reflection image coefficient is a function of the orientation φ of the polarizer.

As explained in section (3.1.1), four (4) surface reflectance images were captured. These images are vectorized into row vector, x_M , where M is the number of captured images. The observation matrix X is composed of these row vectors:

$$X = \begin{bmatrix} x_1 \\ x_2 \\ \dots \\ x_M \end{bmatrix} \tag{3.8}$$

The matrix S composed of two components, d and s, to be row vectors representing diffuse and specular reflection of images:

$$S = \begin{bmatrix} d \\ s \end{bmatrix} \tag{3.9}$$

From equation (3.7) the mixing matrix A is represented as:

$$A = \begin{bmatrix} 1 & f(\varphi_1) \\ 1/2 & f(\varphi_2) \\ \dots & \dots \\ 1/2 & f(\varphi_M) \end{bmatrix} \tag{3.10}$$

For separating the diffuse and specular components, the observation matrix X is decomposed into a product of two matrices, A and S. Since the rank of A and S is 2, the rank of $A \cdot S$ should be 2.

$$X = AS. \tag{3.11}$$

Thus, X was approximated by a matrix of rank 2 and decomposed into a product of two matrices by using the Singular Value Decomposition (SVD). The matrix X after decomposition is represented as:

$$X = UDV^T \tag{3.12}$$

Where U and V are orthogonal matrix and D is the singular matrix of X. In order to maintain equal dimensions between decomposed and desired matrices, a 2×2 non-singular matrix W is introduced. So, the desired decomposition is illustrated as follows:

$$X = \underbrace{UW}_{A} \ \underbrace{W^{-1}}_{S} DV^T. \tag{3.13}$$

Matrices A and S are both expressed by W and now the is to determine W:

$$W = \begin{bmatrix} a & c \\ b & d \end{bmatrix}. \tag{3.14}$$

From equation (3.10), it depicts that the first column of A is a constant vector. W is selected in order to make the first column vector as close as possible to the constant vector. Since the column vectors of U are orthogonal, hence, the value of a and b can be determined and the minimization inversion is solvable:

$$\begin{bmatrix} a \\ b \end{bmatrix} = U^T \begin{bmatrix} 1 \\ . \\ . \\ 1/2 \end{bmatrix}. \tag{3.15}$$

Now, c and d can be determined. Given that W orthogonal and non-singular, its formation can be assumed to be expanded to:

$$W = \begin{bmatrix} a & c \\ b & d \end{bmatrix} = \begin{bmatrix} r_1 \cos\alpha & r_2 cos\beta \\ r_1 sin\alpha & r_2 sin\beta \end{bmatrix}, \tag{3.16}$$

Where r_1 and r_2 are two positive value and r_1 and α are already determined. To determine r_2 and β, the determine Δ of W is

$$Det(W) = \Delta = ad - bc = r_1 r_2 \sin(\beta - \alpha)\ . \tag{3.17}$$

Whose absolute value is in correspondence to the intensity of the specular reflection image. For separating the specular reflection, the determinant was set $|\Delta| = 1$ (always equal to positive) without losing its generality. since r_1 and α are known, if either r_2 and β is

determined, the other one is determined as well. As a result, the value of β was set to gradually change within the range $0 \leq \beta \leq \pi$ and the diffuse and specular reflection images were compute using matrix S from equation (3.13). The minimum mutual information $I(\boldsymbol{d}; \boldsymbol{s})$; between them was computed as indicated by equation (3.18) using their histograms; $\{p(x_i)\}$ and $\{p(y_j)\}$ for diffuse and specular reflection images respectively.

$$I(\boldsymbol{d}; \boldsymbol{s}) = \sum_{i=1}^{L} \sum_{j=1}^{L} p\left(x_i, y_j\right) \log \frac{p(x_i, y_j)}{p(x_i)\, p(y_j)} \qquad (3.18)$$

Where $\{p(x_i, y_1)\}$ represent their joint histogram.

3.3 Surface Normal Estimation

Generally, the degree of polarization DoP is used for shape recovery. DoP is presented in accordance with the I_{max} and I_{min} **[50]** and can be written as:

$$DoP = \frac{I_{max} - I_{min}}{I_{max} + I_{min}} \qquad (3.19)$$

Where I_{max} and I_{min} represents the observed maximum and minimum pixel brightness during the rotation of the polarizer. Since the surface of the observed image is non-Lambertian i.e., it contains reflection of both diffuse and specular reflection, stemming from equation (3.7) the observed polarization images I_{max} and I_{min} can be expressed as:

$$\begin{cases} I_{max} = f_b \cdot I_{max}^{spec} + I_{max}^{diff} \\ I_{min} = f_b \cdot I_{min}^{spec} + I_{min}^{diff} \end{cases} \qquad (3.20)$$

Where the superscripts $diff$ and $spec$ depicts diffuse and specular reflection and the coefficient f_b balances the difference in intensity between diffuse and specular reflection. Substituting the Fresnel equations **[51]** into equation (3.19), the DoP can be expressed as:

$$DoP = \frac{(n - {}^{1}/_{n})^2 \, sin^2\theta}{2+2n^2 - (n + {}^{1}/_{n})^2 sin^2\theta + 4cos\theta\sqrt{n^2 - sin^2\theta}} \tag{3.21}$$

Where n depicts the refracted index and θ is the zenith angle. For this thesis, the refracted index is set to be 1.4. Basically, surface normal estimation is reliant on the zenith (θ) and azimuth angle (ϕ). According to Fresnel's law, Angle of Polarization (AoP) can be estimated as **[2]** shown below:

$$AoP = \frac{1}{2}\arctan\left(\frac{I_0 + I_{90} + 2I_{45}}{I_{90} - I_0}\right) = \phi - 90^{\circ} \quad if\ (I_{90} < I_0) \tag{3.22}$$
$$[if\ (I_{45} < I_0)\ \emptyset = AoP + 180^{\circ}\ \ else\ \ \phi = AoP]$$

Where I_0, I_{45} and I_{90} are the images observed with a polarizer oriented at $0^{\circ}, 45^{\circ}$ and 90° respectfully to a chosen reference orientation.

3.3.1 Correcting Normal from Intensity Information

In order to recover the shape of the object, the $2N^2$ unknowns (θ, ϕ) was accurately determined from equation (3.21) and (3.22) directly from the polarization images. $\boldsymbol{G^{polar}}$ is then calculated from the equation below:

$$G^{polar} = \{grad^{polar}(x).\ grad^{polar}(y)\},$$
$$grad^{polar}(x) = \tan\theta \cos\phi \tag{3.23}$$
$$grad^{polar}(y) = \tan\theta \sin\phi$$

Due to the arctangent function in equation (3.22), it results in multi-valued ϕ, that is the azimuth ambiguity. In shape from polarization, ambiguities have been a major problem. It is an essential problem that fails shape recovery in (3.22). It gives an incorrect estimation of the surface normal which leads to deformity of the recovered 3D information. The multi-valued ϕ results to two different surface normal N and N_s in opposite directions due to the arctangent function in equation (3.22). Only of these two normal is correct and the final accurate normal cannot be determined by only the AoP information.

In order to determine the unique accurate normal, an additional constraint was added to the azimuth, that is, the normal direction. From the separated diffuse image, Lambert cosine law **[52]** was employed to convert the intensity data into height data as shown below:

$$f\left(g_{m,n}^{depth}\right) = I_{m,n} - R\left(grad^{depth}(x), grad^{depth}(y)\right) = 0$$

$$\begin{cases} grad^{depth}(x) = \frac{\partial g_{m,n}^{depth}}{\partial x} = g_{m,n}^{depth} - g_{m,n-1}^{depth} \\ grad^{depth}(y) = \frac{\partial g_{m,n}^{depth}}{\partial y} = g_{m,n}^{depth} - g_{m-1,n}^{depth} \end{cases} \tag{3.24}$$

Where R indicates the reflectance function, $g_{m,n}^{depth}$ depicts the surface height, m and n are the pixel position in X and Y directions, respectively, and the gradient field derived from the image intensity is $G^{depth} = \{ grad^{depth}(x), grad^{depth}(y)\}$.

Therefore the G^{depth} was used as a reference gradient field for the correction of the perturbed gradient filed G^{polar} derived from polarization by using an optimization function as illustrated below:

$$\hat{A} = \arg\min \| G^{depth} - A(G^{polar}) \|_2^2 , \; A \epsilon \{1, -1\} \tag{3.25}$$

Where A is binary operator and $\hat{A}$ is a set of binary operands. The estimated azimuth is accurate if A = 1, and if $A = -1$, removal of ambiguity is required by changing the

direction of the estimated surface normal by changing ϕ into ϕ + π. The implementation of the correction was done by:

$$G^{cor} = A \cdot G^{polar} \quad (3.26)$$

Therefore, with the additional constraint G^{depth} to direction of G^{polar}, the azimuth is addressed.

For the final accurate surface estimation (Z), the global Frankot-Chellappa method was adopted to recover the surface **[53].** The idea behind this method is to construct the integrable surface from the gradient information.

Chapter 4

Results and Discussions

This section shows the results of the steps taken during the implementation of the proposed method as explained in the previous chapter and also discussion on the outcomes of the results.

As explained in section (3.1), a tea cup was the object used for acquiring the polarization images, in which four polarized images were captured. A LED light source was used to provide unpolarized illumination on the surface of the object. These four observed polarized images were the only raw data used in this study for the surface shape recovery. The four raw images are shown below:

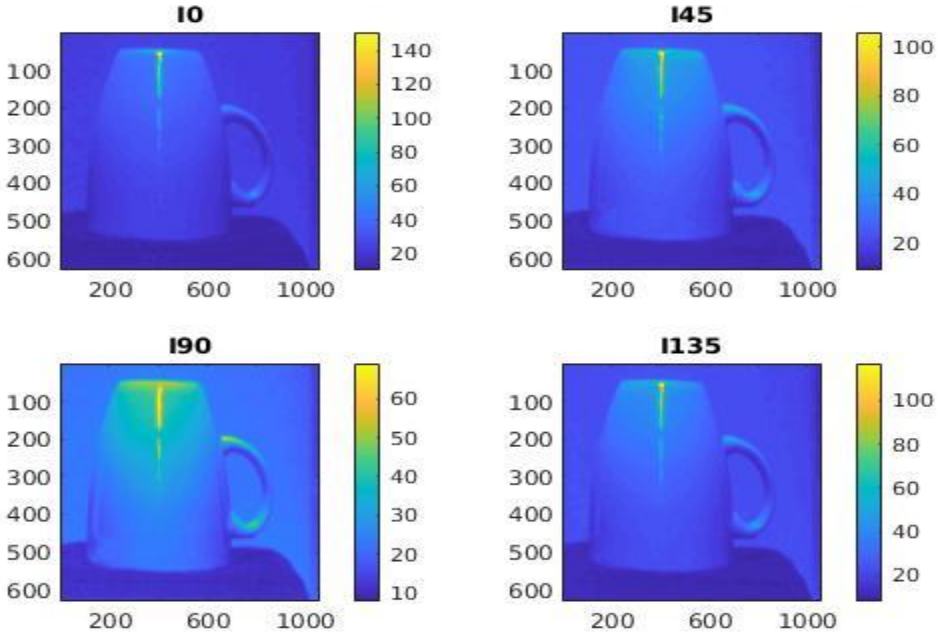

Figure 4.1: Showing the polarized raw intensity images with diffuse and specular reflection.

The proposed separation algorithm of the mixed reflection was applied to the four observed raw polarized raw images. As discussed in section (3.2.1), the mutual information between the two-row vector of S is plotted in Figure (4.2) when β in equation (3.17) varies from 0 to π. The plot shows that the true separation of the specular and diffuse reflection is achieve when β= 2.89. The plot also depicts that the β value achieving the minimum of the mutual information approaches the true value.

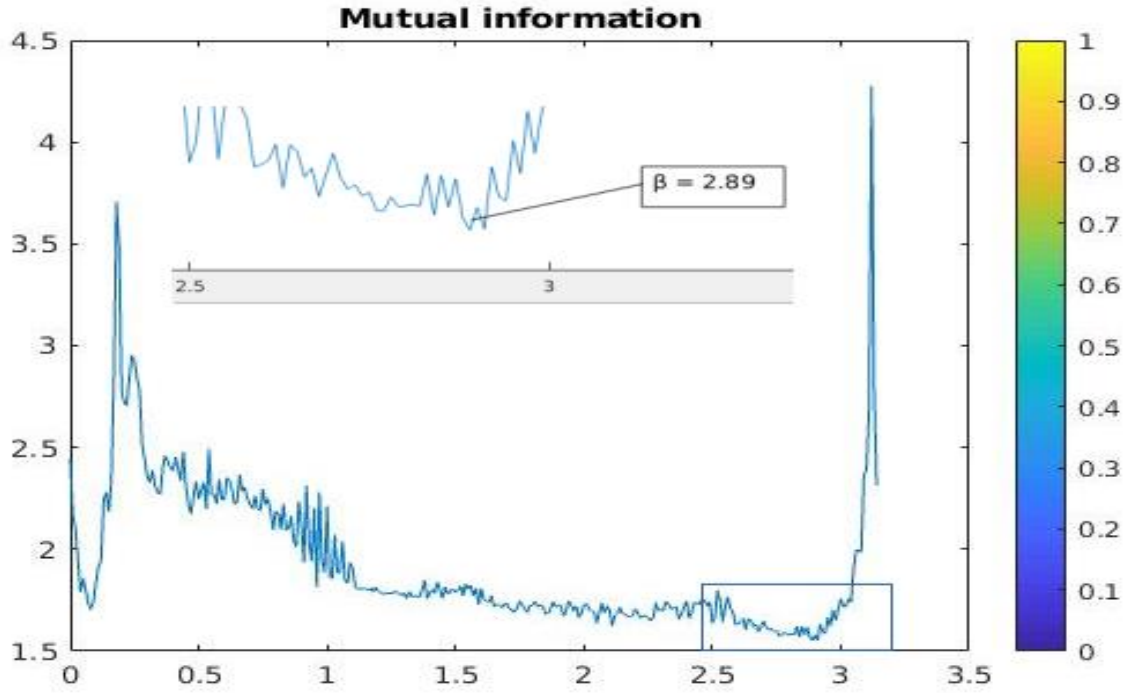

Figure 4.2: Mutual information

The illustration in Figure (4.3) shows the separation algorithm is quite effective but the results is not good enough. The separated specular reflection (b) is well achieved while the separated diffuse (a) still has the presence of specular reflection. This could be as a result of strong intensity of specularity due to the texture of the object material or the illumination from the LED light source.

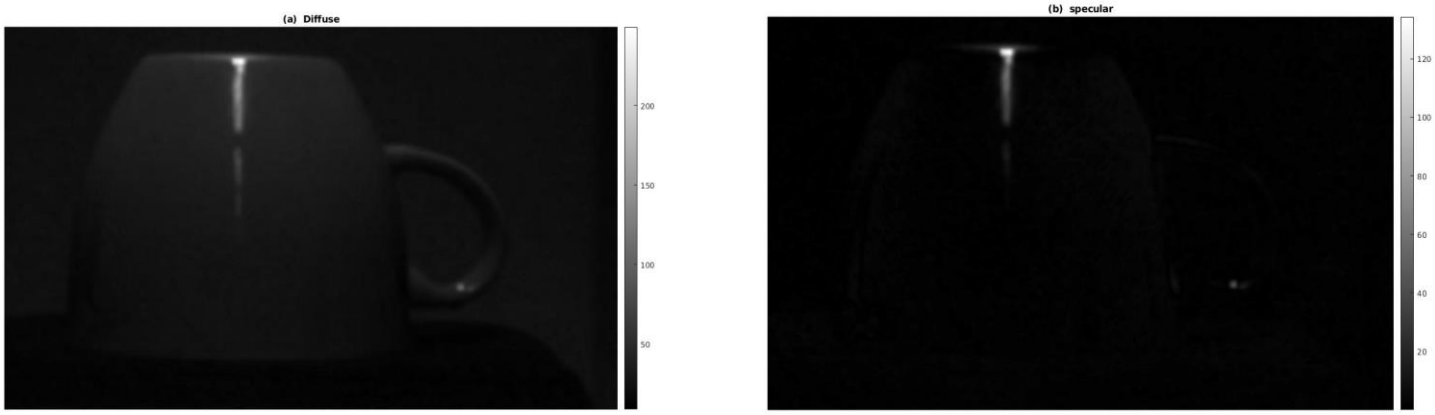

Figure 4.3: (a) Separated diffuse image (b) Separated specular image

As explained in the previous section (3.3), shape recovery from the normal field is determined by the azimuth (ϕ) and zenith angles (θ) in which can be derived by utilizing the Angle of polarization (AoP) and the Degree of Polarization (DoP) Figure (4.3). The result shows lots of noise during the estimation. A smoothing filter was applied which improves the result a little but smoothing has a rapid limit. Based on accurate determination of (θ, ϕ), gradient polar (G^{polar}) Figure (4.4) is first estimated from equation (3.23).

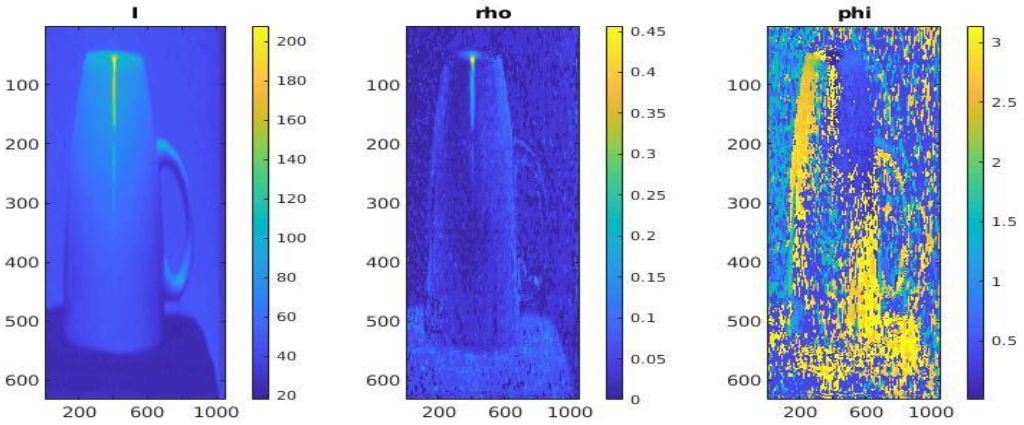

Figure 4.4: Stokes parameters where (I) is the total intensity, (rho) is the Degree of Polarization and (phi) is the Angle of Polarization.

From the (G^{polar}) Figure (4.5), it depicts that the surface of the object is very rough and noisy. This could be a result of the texture of the material or the source of the illumination of light probably the intensity coming from the LED is very strong.

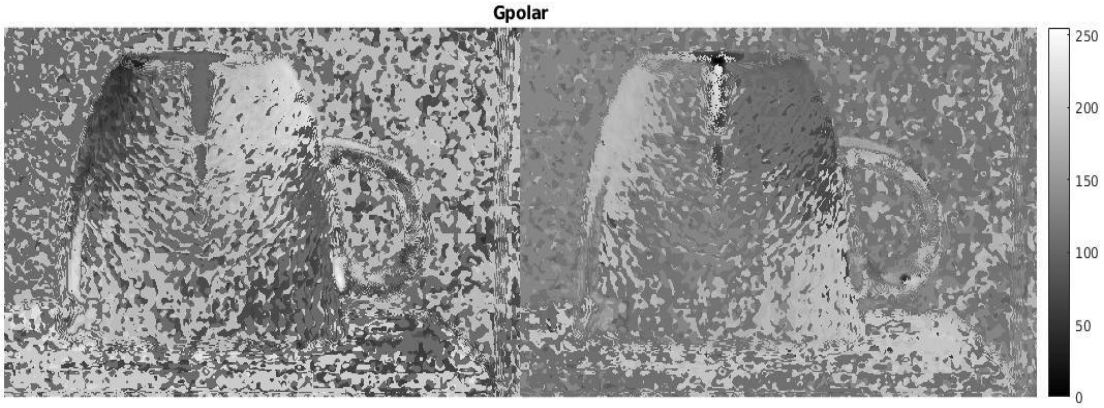

Figure 4.5: Gradient from Polarization (G^{polar}).

As previously explained, the major problem with shape from polarization is ambiguities. The azimuth ambiguity fails the shape recovering due to the arc-tangent function stemming from equation (3.22), which results to in multi-valued (ϕ). This results to error in estimating surface normal due to the surface having two different normals. Only one of these two normals is correct.

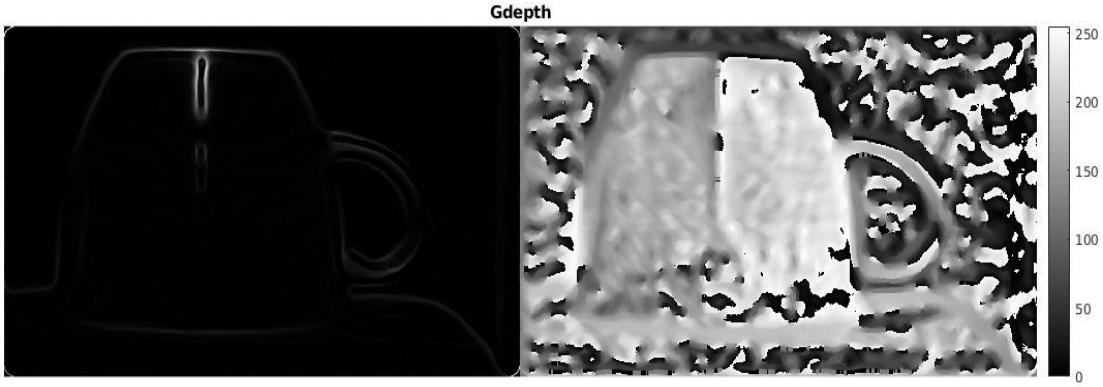

Figure 4.6: Gradient depth from the diffuse separated image (G^{depth})

In order to accurately determine the unique accurate normal, an additional constraint was required to the normal direction. Stemming from equation (3.24), Lambertian reflectance model was employed to covert the intensity data i.e., the diffuse separated data into height data, and then obtained the gradient filed data (G^{depth}) as shown in Figure (4.6) and (4.7) respectively.

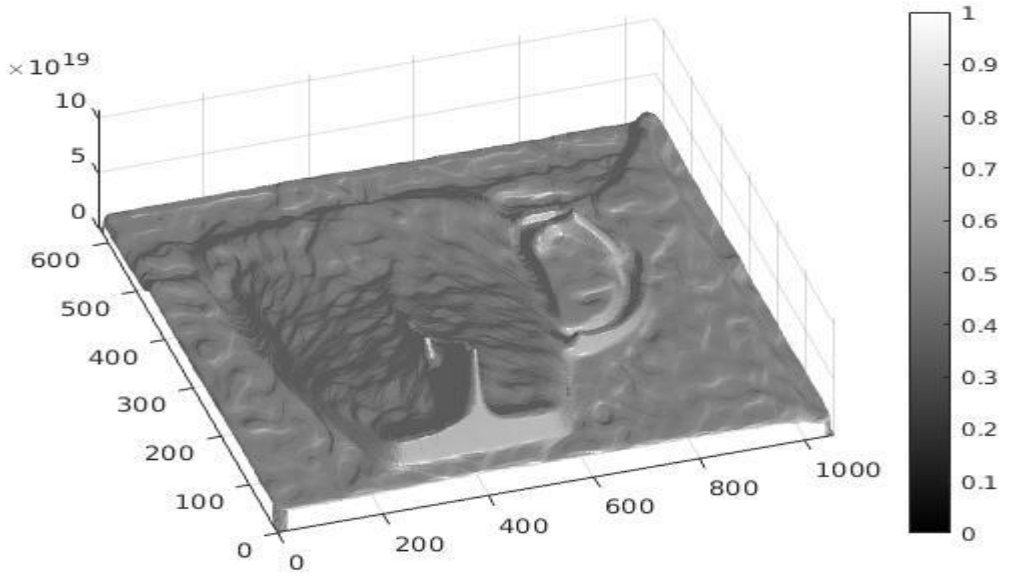

Figure 4.7: Visualizing surface from Gradient depth

Basically, the G^{depth} is to accurately locate the direction of the surface normal at each pixel. Therefore, the G^{depth} was used as a reference gradient field for the correction of the ambiguous gradient filed G^{polar} derived from polarization by using optimization function from equation (3). The result of the corrected gradient ($G^{correct}$) shown in Figure (4.8).

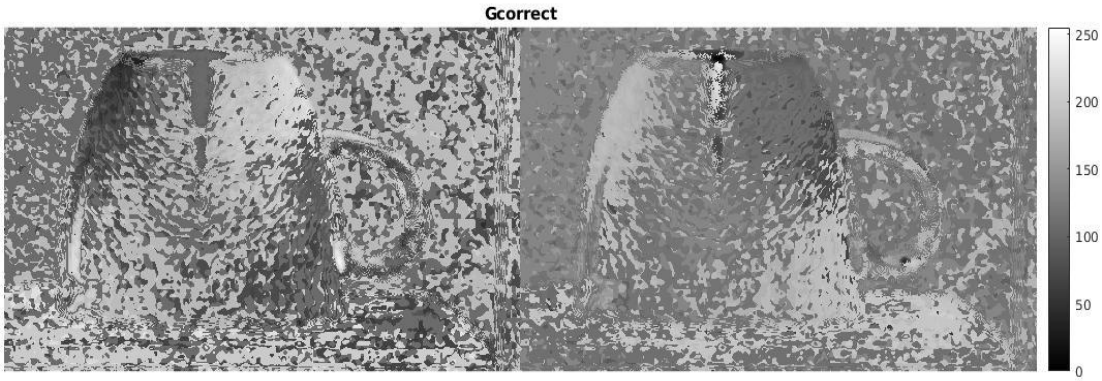

Figure 4.8: Gradient Correction ($G^{correct}$).

Stemming from Franktot-Chelappa global method as explained in section (3.3.1), the method was used for the final accurate surface recovery. The Figure (4.8) depicts the estimation of the final surface normal before correction directly from G^{polar} and after the correct from $G^{correct}$. From the Figure (4.7), the surface gradient depth shows the results is flat. This could be as a result of why there isn't much difference in the final surface normal as shown in Figure (4.8), that is, it basically depicts that the pixel-by-pixel estimation for the correction ($G^{correct}$) very is minimal.

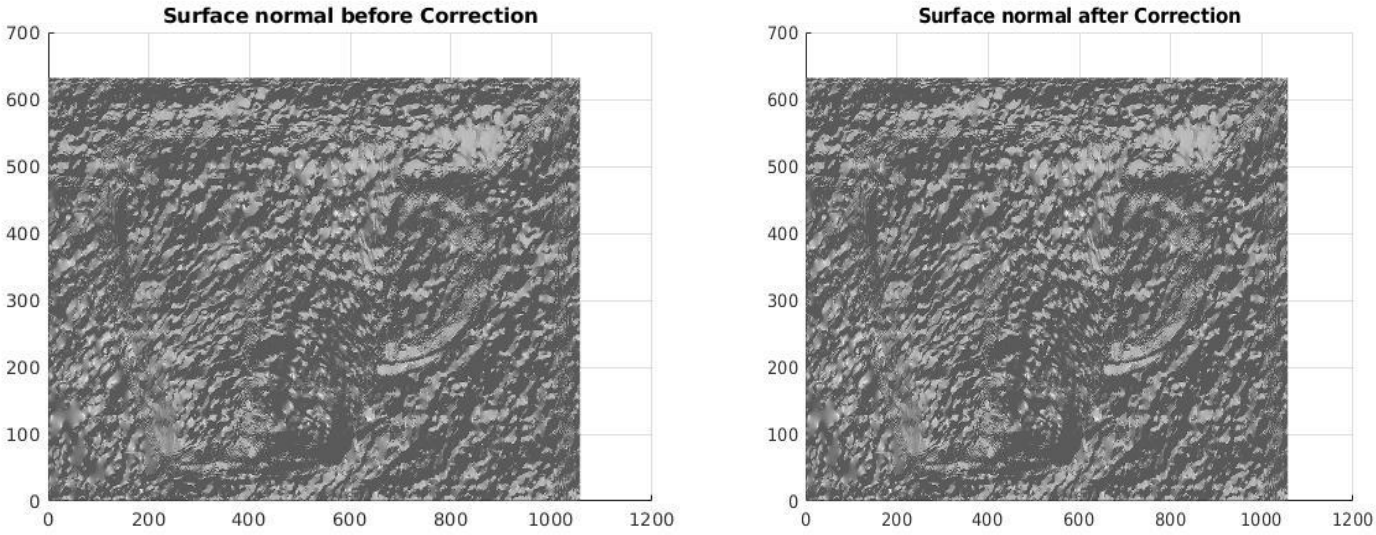

Figure 4.9: On the left, the final surface before correction and on the right, the final surface after correction.

4.1 Comparison with Illumination from the Room Light Source

A comparison was done with four polarization images observed from the room light source. The idea is to show another result from another illumination light source and see the impact of the proposed method on it. From observation in Figure (4.9), it is observed that the intensity of the light on the surface of the object is more evenly distributed compare to the LED light source and the presence of specularity is minimal.

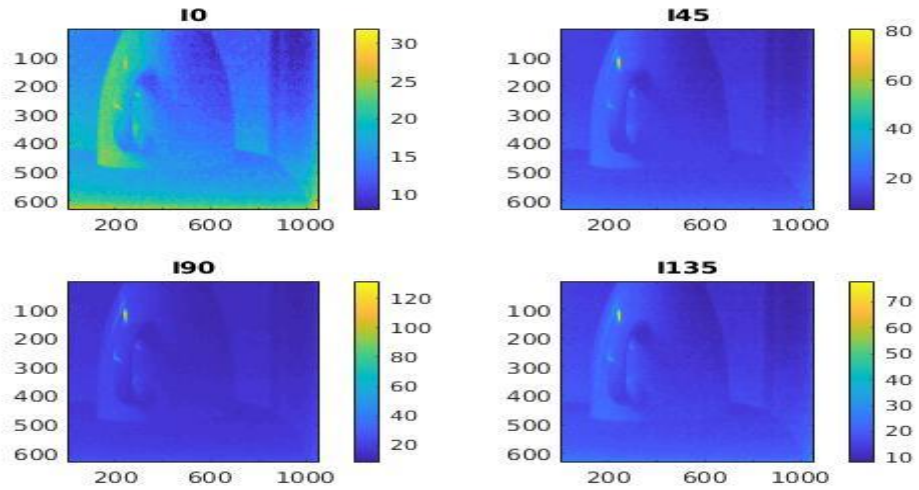

Figure 4.10: polarized images observed from room light source.

The mutual separation almost achieves same results during separation because β value achieving its minimum also close to the true value. This shows the performance of the technique is quite effective. The separated results in Figure (4.10) shows that the separation of the specular was also well achieved and the diffuse still contains presence of specularity but the intensity is minimal.

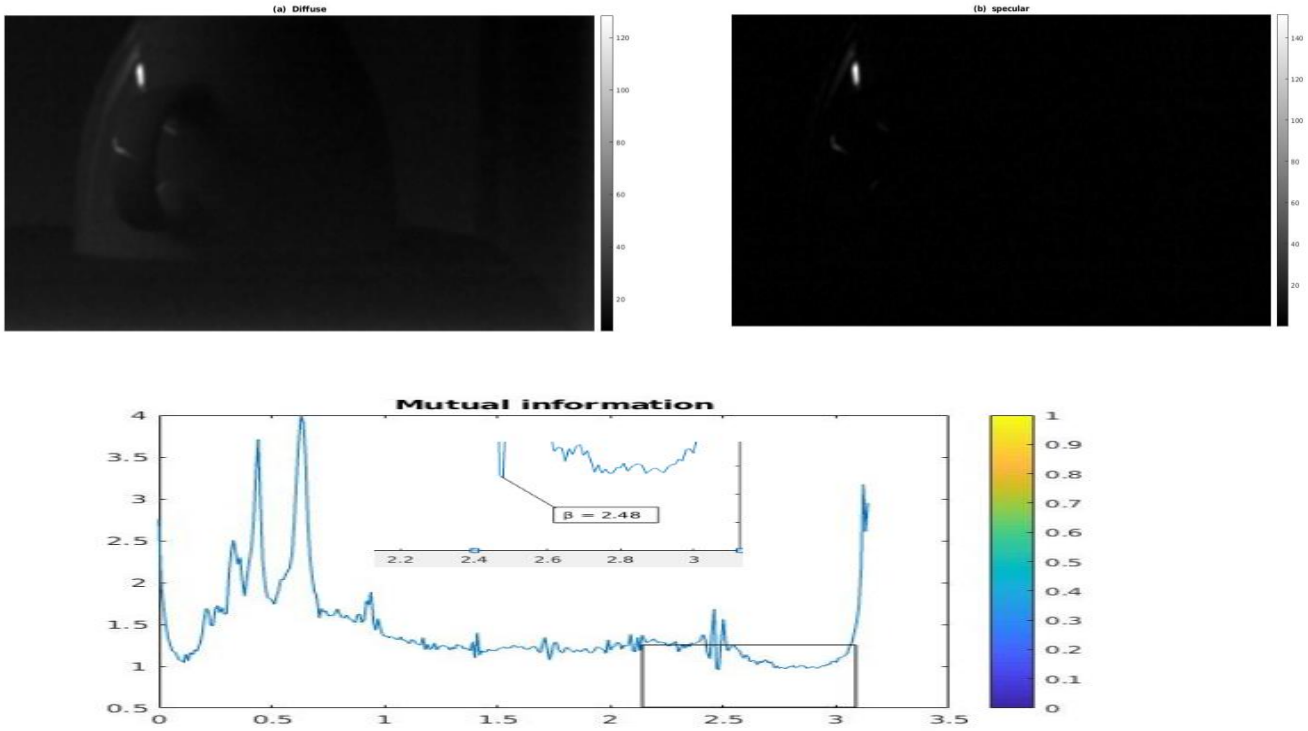

Figure 4.11: At the top, shows the separated polarized mixed reflectance images from the room light source, diffuse and specular respectively and the mutual information plot.

The G^{polar} as shown in Figure (4.12) depicts a very noise surface. The object can be barely seen based on the presence of noise. Compare to the light source from the LED, the noise is lesser. This might be a result of the intensity of the illumination from the room light which is minimal compare to the LED light source.

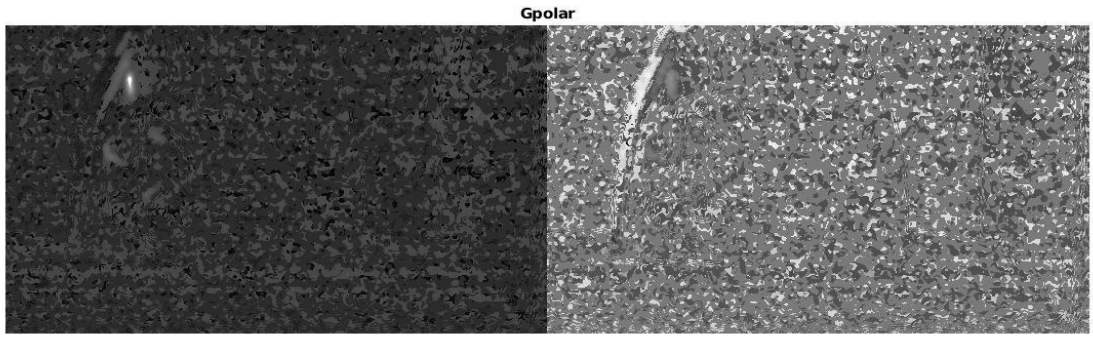

Figure 4.12: Gradient from Polarization

The G^{depth} shows that the surface is also flat but the shape recovery has the presence of concavity compare to the LED illumination.

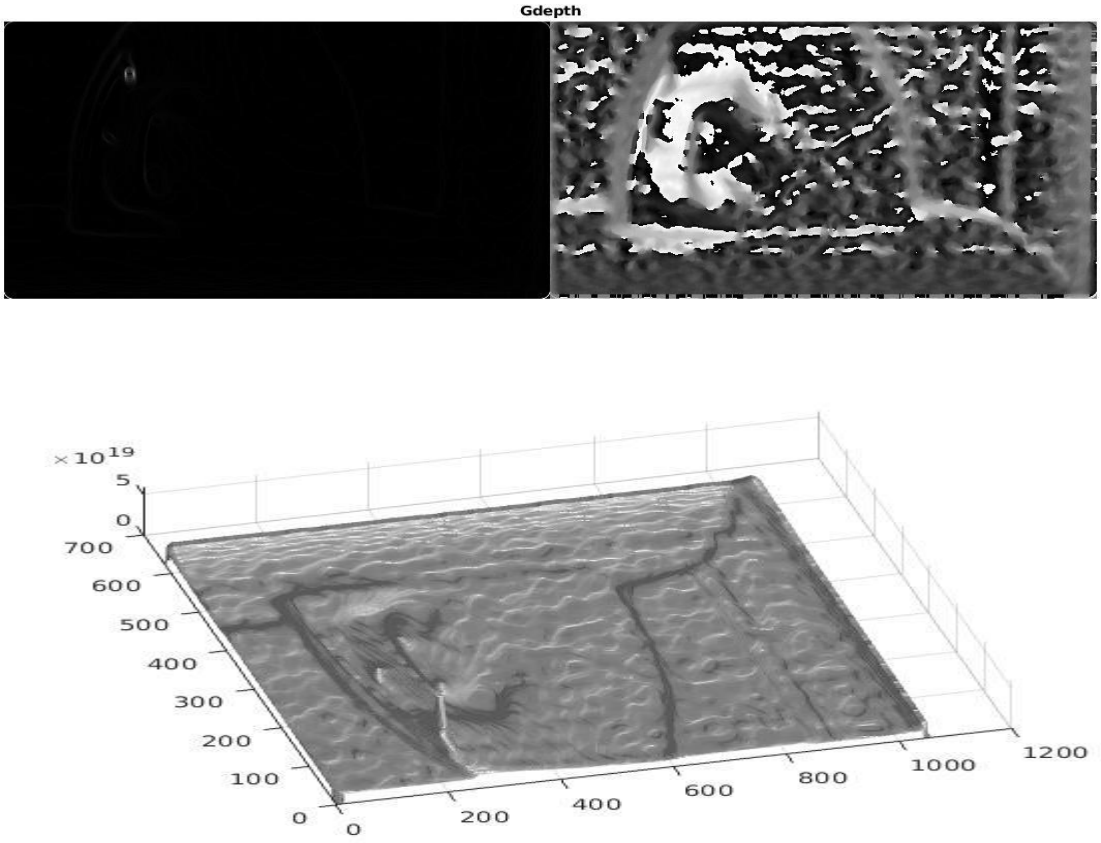

Figure 4.13: Gradient depth and surface from Gradient depth

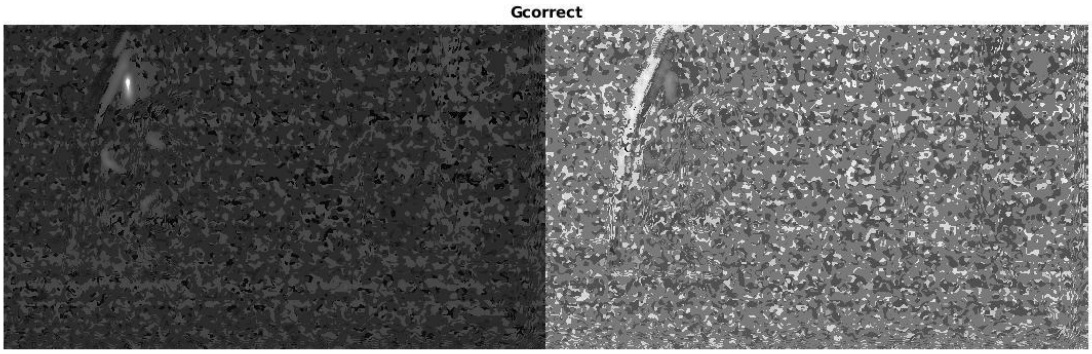

Figure 4.14: Gradient Correction

The $G^{correct}$ (see Figure 4.14) basically shows a result with minimal or no correction from the G^{polar}. For the final surface recovery, the shape is barely seen both from G^{polar} and $G^{correct}$. This could be as a result of the impact of the illumination on the surface of the object.

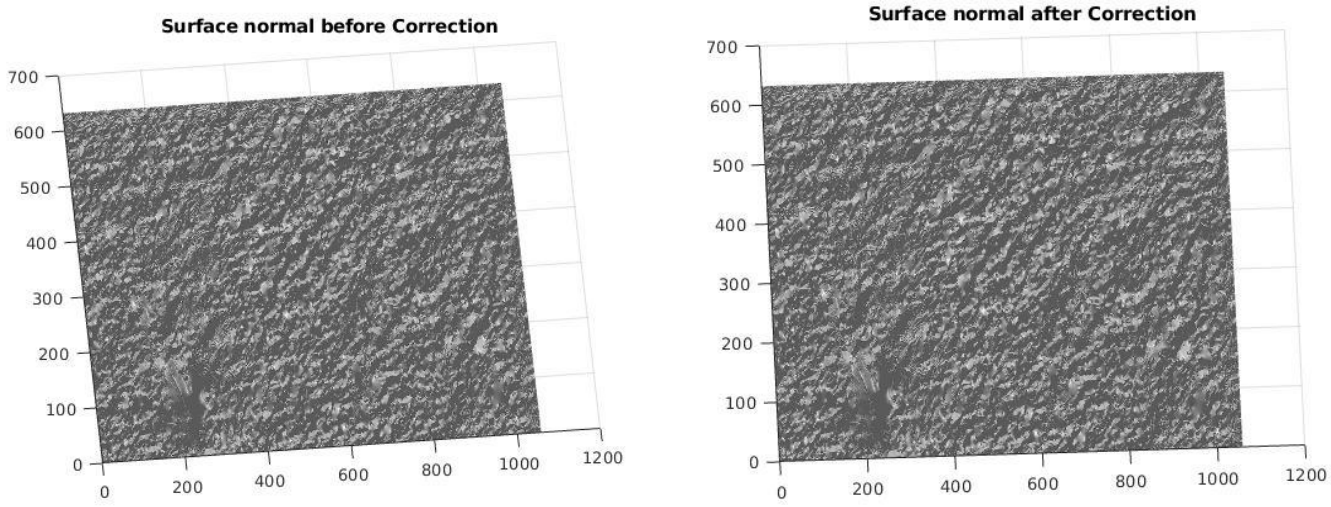

Figure 4.15: Gradient depth and surface from Gradient depth

Chapter 5

Conclusion

In this thesis, a monocular shape recovery method based on polarization properties was introduced. Generally, various shape extraction techniques rely on surface reflection conditions, either pure diffuse or specular reflection. It is more difficult to determine with a non-Lambertian surface because of presence of mixed reflection. The proposed method is featured by two major contributions: separation of mixed reflection and disambiguating azimuth. The idea is to locate and remove specular components from mixed reflection and do accurate estimation with the diffuse components by making it possible for shape recovery of non-Lambertian surfaces. It computes pixel-to-pixel normal gradient field in which solves the normal azimuth ambiguity by providing a correcting reference.

The aim of this thesis was not fully achieved. This is as a result of time constraints to actively seek for more information in order to fully develop the proposed algorithms. The separation of the specularity was well achieved but the pure separated diffuse reflectance was not accurately achieved. This affects the estimation of the surface recovery as seen in the results.

Future work would explore, first the completion of the proposed method in order to achieve the aim of this thesis and secondly to experiment the proposed method to recover shape information from different illumination scene or surface, for instance illumination from a natural condition or recover shape information from a liquid metal surface.

References

[1] B.-Q. Sun, M.-P. Edgar, R. Bowman, L.-E. Vittert, S. Welsh, A. Nowman, M.-J. Padgett, 3D computational imaging with single-pixel detectors. Science 340, 844- 847 (2013).

[2] R. Prevedel, Y.-G. Yoon, M. Hoffmann, N. Pak, G. Wetzstein, S. Kato, T. Schrodel, R. Raskar, M. Zimmer, E.-S. Boyden, A. Vaziri, Simultaneous wholeanimal 3D imaging of neuronal activity using light-field microscopy. Nat. Methods 11, 727-730 (2014).

[3] K. Morimoto, A. Ardelean, M.-L. Wu, A.-C. Ulku, I.-M. Antolovic, C. Nruschini, E. Charbon, Megapixel time-gated SPAD image sensor for 2D and 3D imaging application. Optica 7, 346-354 (2020).

[4] X.-F. He and N. O (2012). Time delay integration speeds up imaging. Photonics Spectra, Vol. 46, Issue 5, pp. 50-54.

[5] D. Miyazaki, R.-T. Tan, K. Hara, K. Ikeuchi, Polarization-based inverse rendering from a single view. In proc. IEEE International Conference on Computer Vision (ICCV) 2, 982-987 (Nice, France, 2003).

[6] L. B. Wol and T. E. Boult. Constraining object features using a polarization reflectance model. IEEE Transactions on Pattern Analysis and Machine Intelligence, 13(7):635{657, 1991.

[7] G. A. Atkinson and E. R. Hancock. Recovery of surface orientation from di use polarization. IEEE Transactions on Image Processing, 15(6):1653{1664, 2006.

[8] S. Rahmann and N. Canterakis. Reconstruction of specular surfaces using polarization imaging. In Proc. CVPR, volume 1, pages I{I, 2001.

[9] F.-Q. Li, H.-J. Chen, A. Pediredla, C. Yeh, K. He, A. Veeraraghavan, O.Cossairt, CS-ToF: high-resolution compressive time-of-flight imaging. Opt. Express 25, 31096-31110 (2017).

[10] S. Heist, C. Zhang, K. Reichwald, P. Kühmstedt, G. Notni, A. Tünnermann, 5D hyperspectral imaging: fast and accurate measurement of surface shape and spectral characteristics using structured light. Opt. Express 18, 23366-23379 (2018).

[11] J.-H. Sun, Y. Zhang, X.-Q. Cheng, A high precision 3D reconstruction method for bend tube axis based on binocular stereo vision. Opt. Express 3, 2292-2304 (2019).

[12] D. Mo, R. Wang, N. Wang, T. Lv, K.-S. Zhang, and Y.-R. Wu, Three-dimensional inverse synthetic aperture lidar imaging for long-range spinning targets. Opt. Lett. 4, 839-842 (2018).

[13] Wolff LB. Relative brightness of specular and diffuse reflection. Opt Eng 1994;33(1):285–93 Jan.

[14] E. Bartholinus and W. Brandt. Experiments with the double refracting Iceland crystal: which led to the discovery of a marvelous and strange refraction. 1959.

[15] C. Hoffman and R. Driggers. Encyclopedia of Optical and Photonic Engineering, Second Edition. CRC Press 2015, 2015.

[16] E. Hecht. Optics. Pearson Education India, 2012.

[17] E. Collett. Field guide to polarization. 2005.

[18] M. Born and E. Wolf. Principles of Optics. Electromagnetic Theory of Propagation, Interference and Diffraction of Light. Pergamon, London, 1959.

[19] L. B. Wolff, "Polarization-based material classification from specular reflection," EEE Trans. Pattern Analysis and Machine Intelligence 12, pp. 1059–1071, November 1990.

[20] L. B. Wolff, "Polarization vision: a new sensory approach to image understanding," Image and Vision Computing 15, pp. 81–93, February 1997.

[21] L. B. Wolff and A. Andreou, "Polarization camera sensors," Image and Vision Computing 13, pp. 497–510, August 1995.

[22] Konstantin M. Yemelyanova, Shih-Schn Lina, William Q. Luisa, Edward N. Pugh, Jr. b, and Nader Enghetac, "Bio-inspired display of polarization information using selected visual cues", Proceedings of SPIE Vol. 5158 Polarization Science and Remote Sensing, 2003

[23] D. Miyazaki, M. Kagesawa, and K. Ikeuchi, IAPR (IEEE,2002), pp. 26–31.

[24] O. Morel, C. Stolz, F. Meriaudeau, and P. Gorria, Appl. Opt.45, 4062 (2006).

[25] Atkinson, G. A., & Hancock, E. R. (2006). Recovery of surface orientation from diffuse polarization.

[26] M. Ferraton, C. Stolz, and F. Meriaudeau. Surface reconstruction of transparent objects by polarization imaging. In Signal Image Technology and Internet Based Systems, 2008. SITIS ’08. IEEE International Conference on, pages 474 –479, 30 2008-dec. 3 2008.

[27] B. K. P. Horn. Shape from Shading: A Method for Obtaining the Shape of a Smooth Opaque Object from One View. PhD thesis, MIT, 1970.

[28] K. J. Krakauer. Computer Analysis of Visual Properties of Curved Objects. PhD thesis, MIT, 1971.

[29] P. Dupuis and J. Oliensis. Direct method for reconstructing shape from shading. In Proc. CVPR, pages 453–458, 1992.

[30] P. L. Worthington and E. R. Hancock. New constraints on data-closeness and needle map consistency for shape-from-shading. IEEE Trans. Patt. Anal. Mach. Intell., 21:1240–1267, 1999.

[31] P. L. Worthington. Re-illuminating single images using albedo estimation. Pattern Recognition, 38:1261–1274, 2005.

[32] L. B. Wolff, S. K. Nayar, and M. Oren. Improved diffuse reflection models for computer vision. Intl. J. Comp. Vis., 30:55–71, 1998.

[33] H. Ragheb and E. R. Hancock. Surface radiance correction for shape from shading. Pattern Recognition, 38:1574–1595, 2005.

[34] K. Ikeuchi and B. K. P. Horn. Numerical shape from shading and occluding contours. Artificial Intelligence, 17:141–184, 1981.

[35] M. J. Brooks and B. K. P. Horn. Shape and source from shading. In Proc. Intl. Joint Conf. Artificial Intelligence, pages 935–936, 1985.

[36] I. Shimishoni, Y. Moses, and M. Lindenbaum. Shape reconstruction of 3D bilaterally symmetric surfaces. Intl. J. Comp. Vis. 39:97–110, 2000.

[37] R. T. Frankot and R. Chellappa. A method for enforcing integrability in shape from shading algorithms. IEEE Trans. Patt. Anal. Mach. Intell., 10:439–451, 1988.

[38] A. Agrawal, R. Chellappa, and R. Raskar. An algebraic approach to surface reconstruction from gradient fields. In Proc. ICCV, pages 174–181, 2005.

[39] T. Simchony, R. Chellappa, and M. Shao. Direct analytical methods for solving Poisson equations in computer vision problems. IEEE Trans. Patt. Anal. Mach. Intell., 12:435–446, 1990.

[40] A. Robles-Kelly and E. R. Hancock. A graph-spectral method for surface height recovery from needle-maps. In Proc. CVPR, pages 141–148, 2001.

[41] R. White and D. A. Forsyth. Combining cues: Shape from shading and texture. In Proc. CVPR, pages 1809–1816, 2006.

[42] Y. Furukawa and C. Hernandez. Multi-view stereo: A tu- ´ torial. Foundations and Trends in Computer Graphics and Vision, 9(1-2):1–148, 2015.

[43] G. Vogiatzis, P. Torr, and R. Cippola. Multi-view stereo via volumetric graph-cuts. In Proceedings of CVPR, 2005.

[44] K. Kolev, M. Klodt, T. Brox, and D. Cremers. Continuous global optimization in multiview 3d reconstruction. International Journal of Computer Vision, 2009

[45] E. Tola, V. Lepetit, and P. Fua. DAISY: An Efficient Dense Descriptor Applied to Wide Baseline Stereo. IEEE Transactions on Pattern Analysis and Machine Intelligence, 32(5):815–830, 2010.

[46] Pingli Han, Yudong Cai, Fei Liu, Xuan Li, Rongguang Liang, Mingyu Yan, Xiaopeng Shao. Computational polarization 3D: New solution for monocular shape recovery in natural conditions. Optics and Lasers in Engineering 151 (2022) 106925

[47] WolffLB, Boult TE. Constraining object features using a polarization reflectance model. IEEE Trans Pattern Anal Mach Intell 1991;13(7):635–57 Jul.

[48] Born M, Wolf E. Principles of optics: electromagnetic theory of propagation, inter- ference and diffraction of light. Cambridge: Cambridge University Press; 1999.

[49] Umeyama S, Godin G. Separation of diffuse and specular components of surface reflection by use of polarization and statistical analysis of images. IEEE Trans Pattern Anal Mach Intell 2004;26(5):639–47 Mar.

[50] Liu F, Han PL, Wei Y, Yang K, Huang SZ, Li X, Zhang G, Bai L, Shao XP. Deeply seeing through highly turbid water by active polarization imaging. Opt Lett 2018;43(20):4903–6 Oct.

[51] Hecht, E. (2002). Optics (4th ed.). San Francisco: Addison-Wesley.

[52] Basri R, Jacobs DW. Lambertian reflectance and linear subspaces. IEEE Trans Pattern Anal Mach Intell 2003;25(2):218–33 Feb.

[53] Frankot, R.T., Chellappa, R.: A Method for Enforcing Integrability in Shape from Shading Algorithms. IEEE Transactions on Pattern Analysis and Machine Intelligence 10(4), 439–451 (1988)